International Communications in Heat and Mass Transfer 131 (2022) 105753

Contents lists available at ScienceDirect

International Communications in Heat and Mass Transfer

journal homepage: www.elsevier.com/locate/ichmt

Numerical simulation of thermo-magnetic convection and entropy production in a ferrofluid filled square chamber with effects of heat generating solid body

S. Priyadharsini [a,b], C. Sivaraj [a,*]

[a] Department of Mathematics, PSG College of Arts & Science, Coimbatore 641014, Tamil Nadu, India
[b] Department of Mathematics, Sri Krishna Arts and Science College, Coimbatore 641008, Tamil Nadu, India

ARTICLE INFO

Keywords:
Thermo-magnetic convection
Entropy production
Magnetite nanoparticle
Ferroliquid
Heat generating solid body

ABSTRACT

Thermo-magnetic convection and entropy production are the most widely used subjects of study in the field of an effective design tools for cooling electronic devices. The present work focuses on numerical simulation of thermo-magnetic convection cooling of the heat-generating solid block placed in a magnetite suspended nanoliquid filled chamber. The surfaces of the horizontal borders of the chamber are thermally insulated whilst the vertical borders are cooled at a constant temperature. The finite volume technique with a simple algorithm on a uniform staggered grid is employed to transform the governing non-linear PDE into a set of discretized equations. The liquid motion, thermal transmission, and entropy production are discussed for various pertinent parameters such as solid volume fractions of the nano-additive ($\varphi = 0.01 - 0.04$), aspect ratio of a heat-generating solid body ($A_s = 0.25 - 4$), thermal conductivity ratio of the heat generating body ($0.1 \leq k^* \leq 5.0$), Hartmann number ($Ha = 0 - 50$) and irreversibility ratio ($\Omega = 0.001 - 0.1$) . Isolines of temperature, stream function, normalized entropy along with profiles of mean Nusselt number and mean entropy production outcomes are demonstrated graphically. The results showed that reduction in aspect ratio increases the cooling efficiency due to the hindrance-free effect and produces a high heat transfer rate. Minimum entropy production occurs at low thermal conductivity ratio ($k^* = 0.1$) . The thermal performance criterion also justifies that the least aspect ratio manifests better thermal performance.

1. Introduction

Thermal convection cooling in an electronic contrivance with typical inner energy source has become a serious challenge in numerous engineering fields. More details concerning natural convection in a square cavity with heat-conducting and generating obstructions/baffles could be found in the review papers of House et al. [1], Oh et al. [2] and Ha et al. [3], etc.

To reduce the risk of damage or failure of the electronic equipment, analyzing free convection in a chamber having a heat generating solid body is supposed to be one of the promising solutions. It has several applications such as home electric appliances, contractual design, energy storage, heat exchangers and cooling of electronic equipment, etc. Introducing the nanoparticle in the base fluid is one of the best typical passive cooling techniques. Since thermal conductivity of the base fluid is slightly low, addition of nanoparticle providing the effective heat transfer rate due to its improved thermal conductivity. On the other hand, external effect of magnetic field has the potential to control heat transfer and attained better stability in the flow field.

Miroshnichenko et al. [4] explored the significance of alumina-nanoliquid in an open chamber inserted with a heat generating solid body. Thermo-gravitational convection inside an alumina-H_2O filled square chamber having thermally- producing solid body has been analyzed by Bondarenko et al. [5] via heatline visualization technique. The authors reported that an internal energy portion achieves a passive cooling of closed electronic cabinets. Very recently, an optimized stochastic algorithm has been implemented by Nouar et al. [6] to investigate an unsteady nanoliquid flow. Nowadays, additionally incorporated nanoliquid called hybrid-nanoliquid is extremely useful in incipient fields of study. Karimipour et al. [7] examined a significant analysis of $CuFe_2O_4$ suspended by SiO_2 along with H_2O/ethylene glycol in order to make a new homogeneous nanofluid. So far, numerous investigators have been studied related to convection filled by hybrid nanofluids can

* Corresponding author.
E-mail address: vcsivaraj@gmail.com (C. Sivaraj).

https://doi.org/10.1016/j.icheatmasstransfer.2021.105753

Available online 6 January 2022

Nomenclature

Roman letters

A_s	aspect ratio of the solid body (l_1/l_2)
B	strength of magnetic influence ($kg/s^2/amp$)
Be_{Avg}	average Bejan number
c_p	specific heat (J $kg^{-1}k^{-1}$)
g	gravitational acceleration (m s^{-2})
Ge	Gebhart number, $(g\beta_f L/(c_p)_f)$;
Ha	Hartmann number
k	thermal conductivity (W m^{-1} K^{-1})
k^*	thermal conductivity ratio
l_1	dimensional length of the solid body (m)
l_2	dimensional height of the solid body (m)
L	size of the chamber (m)
Nu	local Nusselt number
$\overline{\mathrm{Nu}}$	mean Nusselt number
p	dimensional pressure (N m^{-2})
P	dimensionless pressure
Pr	Prandtl number (ν_f/α_f)
q'''_{gen}	Uniform heat generation rate (Wm^{-3})
Ra	Rayleigh number ($g\beta_f\Delta TL^3/\nu_f\alpha_f$)
s_{gen}	local entropy production (W $K^{-1}m^{-3}$)
$s_{gen,HT,ff}$	local entropy production owing to energy transport in ferrofluid (W $K^{-1}m^{-3}$)
$s_{gen,HT,s}$	local entropy production owing to energy transport in a solid (W $K^{-1}m^{-3}$)
$s_{gen,HT}$	local entropy production owing to energy transport (W $K^{-1}m^{-3}$)
$s_{gen,FF}$	local entropy production owing to liquid friction (W $K^{-1}m^{-3}$)
$s_{gen,MF}$	local entropy production owing to magnetic field (W $K^{-1}m^{-3}$)
S_{gen}	non-dimensional local entropy production
$S_{gen,HT,ff}$	non-dimensional local entropy production owing to energy transport in ferrofluid
$S_{gen,HT,s}$	non-dimensional local entropy production owing to energy transport in a solid
$S_{gen,HT}$	non-dimensional local entropy production owing to energy transport
$S_{gen,FF}$	non-dimensional local entropy production owing to liquid friction
$S_{gen,MF}$	non-dimensional local entropy production owing to magnetic field
$S_{Avg,T}$	non-dimensional mean entropy production
$S_{Avg,HT}$	non-dimensional mean entropy production owing to energy transport
$S_{Avg,FF}$	non-dimensional mean entropy production owing to liquid friction
$S_{Avg,MF}$	non-dimensional mean entropy production owing to magnetic field
t	dimensional time (s)
T_{ff}	dimensional temperature for a fluid region,(K)
T_s	dimensional temperature for a solid region (K)
T_c	dimensional cold wall temperature (K)
u, v	dimensional horizontal and vertical velocities (m s^{-1})
U, V	non-dimensional horizontal and vertical velocities
x, y	dimensional Cartesian coordinates (m)
X, Y	non-dimensional Cartesian coordinates

Greek symbols

α	heat diffusivity (m^2 s^{-1})
β	heat expansion coefficient (K^{-1})
ε	Thermal performance criteria
ν	kinematic viscosity (m^2 s^{-1})
μ	dynamic viscosity (kgm^{-1} s^{-1})
Ω	non-dimensional irreversibility ratio
φ	nano-sized particles volume fraction
ρ	density (kg m^{-3})
(ρc_p)	heat capacitance (J K^{-1} m^{-3})
$(\rho\beta)$	thermal expansion ($10^{-6}K^{-1}$)
Ψ	non-dimensional stream function
σ	electrical conductivity $(\Omega m)^{-1}$
θ_{ff}	non-dimensional temperature for a fluid region
θ_s	non-dimensional temperature for a solid region
τ	non-dimensional time

Subscripts

Avg	average
c	cold
f	fluid
ff	ferrofluid
max	maximum
p	particle
s	solid
sf	surface

be found in Refs. [8,9].

The study of MHD thermal convection has witnessed a fascinating development and still continues to extend in numerous sectors. To reduce the risk of damage or failure of the electronic equipment, analyzing MHD free convection in a chamber is supposed to be one of the promising solutions. For this, thermal transference by employing kerosene/Fe_2O_3 nanoliquid in an oscillating pipe under the influence of magnetic field has been investigated experimentally by Goshayeshi et al. [10]. Goshayeshi et al. [11,12] assessed the effect of magnetic field in a ferrofluid during the thermal transfer process inside the closed-loop heat pipe and pulsating heat pipe respectively.

Very few investigators have been focused on magneto-thermal radiation in a chamber with heat conducting solid body. Saravanan et al. [13] studied the combined impact of thermal radiation and thermal convection on heat transfer within a closed cavity containing a solid body located at its center. The outcomes show that the thermal performance can be more optimal when aspect ratio is reduced. Mikhailenko et al. [14] investigated the notable influence of radiation in thermal cooling process in a rotating cavity with a heat-generating solid body. Mixed convection with the presence or absence of thermal radiation in a lid-driven chamber filled with alumina-H_2O nanoliquid under the effect of heat generating and conducting element has been investigated by Shulepova et al. [15]. They concluded that the thermal radiation parameter, heater location and volumetric nanosuspension of alumina nanoliquid lead to achieve more effective heat transference. Impact of thermal radiation on free convective heat transport in an inclined chamber within a centered thermally-producing solid block was examined by Sivaraj et al. [16]. The authors have presented that the thermal transmission across the cavity can be improved with growing the surface emissivity. Nia et al. [17] studied the case of MHD thermal transmission and gas circulation in an inclined chamber with thermally generating hollow block.

Eid et al. [18] studied the variance of heat conductivity and the influence of heat generation on magneto-hybrid nanoliquid flow in a porous medium; they reported that the increasing trend of nanoparticles leads to enhance the heat transfer rate of hybrid nanoliquid. Amine et al. [19] examined $Ag - MgO$/Water hybrid nanoliquid filled in a triangular chamber incorporating a rotating circular obstacle under the influence

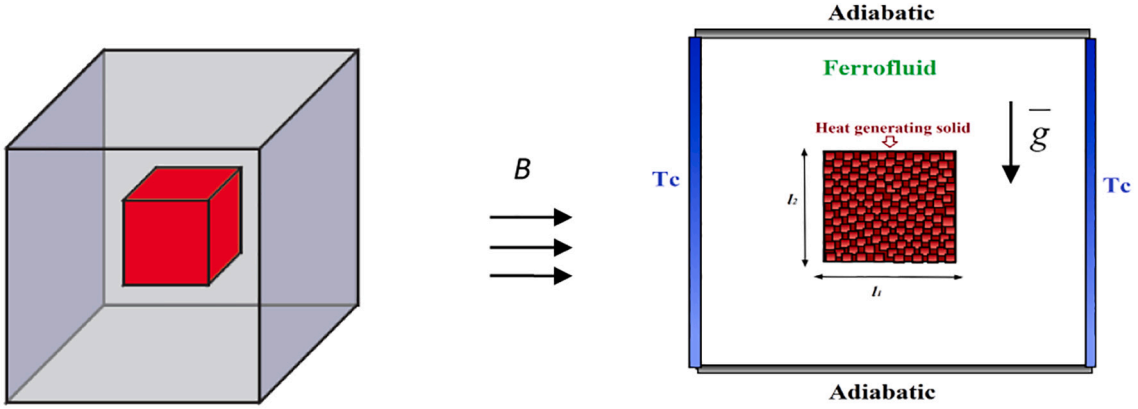

Fig. 1. Physical configuration. **Left:** 3-D view. **Right:** 2-D view.

Table 1
Thermo-physical properties of the base fluid and nanoparticles [50].

Physical properties	Basefluid Water	Ferro-nanoparticle Fe_3O_4
c_p [J kg^{-1} K^{-1}]	4179	670
ρ [kg m^{-3}]	997.1	5200
k [W m^{-1} s^{-1}]	0.613	6
σ [S m^{-1}]	0.05	25,000
$\beta \times 10^{-5}$ [K^{-1}]	20.7	1.18
μ [kg m^{-1} s^{-1}]	0.001003	

of magnetic parameter. Jamshed et al. [20] inspected the consequences of Lorentz force in a driven cavity filled with Powell-Eyring nanofluid. An investigation of Eid et al. [21] showed the effect of electromagnetic in a fluid flow using the Darcy-Forchheimer scheme. Ayeche et al. [22] investigated the impact of transversal magnetic parameter on 2D unsteady hydromagnetic boundary-layer laminar flow of bio-magnetic liquid over a wedge by adopting a micropolar liquid. MHD thermal convection in CNT-based nanoliquid-filled annular circular enclosure with heat-generating solid cylinder is reported by Tayebi et al. [23].

An internal heat generation acknowledged relatively lesser attention from the investigators than that of an external heating. Together with the investigation of entropy production is the most fundamental characteristic in the scrutiny of closed cabinets. Most importantly, the entropy minimization method has an extensive range of applications in industrial and engineering problems and it is commonly adopted techniques for optimizing design parameters. Many investigations have focused related to the process of entropy production and free convections, which is started by Shuja [24], Famouri and Hooman [25] and Sheikholeslami et al. [26].

Therefore, the investigation of entropy production is a primary feature in the review of the successful thermal design. A numerical study of MHD thermal convection associated with entropy production in a ferrofluid filled square chamber having a non-uniformly heated horizontally plate is performed by Sivaraj et al. [27] and reported that average entropy generation can be decreasing trend with enhancing magnetic parameter. Recently, Alnaqi et al. [28] investigated entropy generation, in which the effects of magnetic field with a conducting fin are mainly analyzed. Al-Rashed et al. [29] studied the problem of entropy production and thermal convection of Al_2O_3-nanoliquid inside a chamber with two inclined blades. Bondarenko et al. [30] investigated numerically mixed convection cooling and entropy production of alumina nanoliquid in a square enclosure under the impact of heat conducting and generating solid block with upper moving wall.

Tayebi et al. [31] reported imposing magnetic field effect on a chamber with a corrugated conducting block. The effects of various pertinent parameters including the Rayleigh number, Hartmann number, nanoparticle volume fraction, cavity inclination angle on the thermal and flow field have been analyzed numerically. Parveen et al. [32] employed the bi-conjugate gradient stabilized (Bi-CGStab) method to scrutinize the impact of magnetic effect in a wavy cavity saturated with alumina nanoliquid. Li et al. [33] analyzed both magnetic and radiation effects within an inclined chamber having a circular baffle in terms of entropy generation. Sivaraj et al. [34] show the importance of the entropy generation minimization technique by analyzing the irreversibility in a ferrofluid-filled chamber equipped with a hot rectangular solid block. O. Cicek et al. [35] inspected entropy analysis on the conjugate forced convection phenomena in a semi-cylindrical enclosure with airflow. Recently, O. Cicek et al. [36] utilized entropy minimization as a crucial tool to explore the optimization by analyzing the mixed convection of SWCNT-H_2O nanoliquid in an annulus partially filled with a porous layer. Sivaraj et al. [37] investigated MHD thermo-gravitational energy transport and entropy production in a square chamber saturated with ferric oxide nanoliquid equipped with a vertical hot sheet.

None of the prevailing studies explicitly deal with the effect of heat-generating solid body on thermal convection and entropy production, despite their significance in engineering applications. Many reported studies on entropy generation of the permeable medium can be found by assuming that both phases are thermally identical. Therefore, one of the major goals of this study is to predict and control the temperature distributions inside thermally-producing solid body with the help of entropy production minimization technique, which can give a better design for electronics cooling. The corresponding thermal irreversibility function was suggested using a differential model by Hosseini et al. [38]. A very few numerical studies can be established in the applications of industrial and engineering sectors such as ceramic industry [39], oil extraction [40] and solar thermal applications such as solar aircraft [41] and solar energy [42], etc.

Depending on the literature survey presented above, the object of the present study aims to explore the major characteristics of heat-generating solid body on the thermal convection and entropy production in a chamber under the influence of a magnetic field. The novelty of this work is that two-dimensional temperature distributions and thermal entropy production function of both solid and fluid phases are obtained independently. The effect of thermal conductivity ratio, aspect ratio, and irreversibility ratio is scrutinized. The underlying physical significance of solid-phase heat generation in entropy production is elucidated also the presented work could provide an effective design tool to control heat accumulation in electronic equipment.

2. Mathematical formulation

In this study, MHD thermal convection and entropy production in an enclosure of length L, equipped with a centrally placed heat-generating

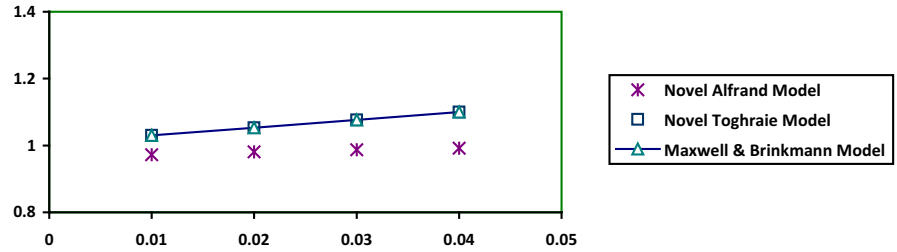

Fig. 2. Comparison of average Nusselt number with different φ for Maxwell [44] & Brinkmann [45], Afrand [47] and Toghraie [49] model for $A_s = 1.0$.

Table 2
Comparison of mean Nusselt Number with House et al. [1].

Ra	ς	k^*	House et al. [1]	Present outcomes	Error %
10^5	0.5	0.2	4.624	4.6353	0.24
10^5	0.5	1	4.506	4.5131	0.16
10^5	0.5	5	4.324	4.3266	0.06
10^6	0.9	0.2	2.402	2.4354	1.39
10^6	0.9	5	3.868	3.8200	1.25

solid body of different aspect ratio is considered (see Fig. 1). The external surfaces of the horizontal borders of the chamber are thermally insulated, whilst the external borders of the others are kept at a fixed cold temperature T_c. It is assumed that an internal solid body is generating heat at a uniform rate q'''_{gen} and also its area is maintained to be $L^2/9$. The flow driven by temperature gradient is assumed to be two-dimensional and laminar. The base fluid and the nanoliquid are in thermal equilibrium and its properties are assumed to be constant (see Table 1) excluding the density in the buoyancy term. Ferrofluid is Newtonian, incompressible and Boussinesq approximation is applicable. A uniform magnetic field of strength B is enforced in the horizontal direction, which affects the flow movement and the induced magnetic field can be ignored related to the applied magnetic field. Further, it is assumed that the viscous dissipation and radiation effects are neglected. Accordingly, the offered configuration will give a good approximation to choose effective geometrical parameters to design the thermal system from the energy-saving point of view.

With the aforementioned assumptions, the governing equations for conservation of mass, momentum and energy can be inscribed in the dimensional form as follows: [16]

$$\frac{\partial u}{\partial x}+\frac{\partial v}{\partial y}=0 \tag{1}$$

$$\rho_{ff}\left(\frac{\partial u}{\partial t}+u\frac{\partial u}{\partial x}+v\frac{\partial u}{\partial y}\right)=-\frac{\partial p}{\partial x}+\mu_{ff}\left(\frac{\partial^2 u}{\partial x^2}+\frac{\partial^2 u}{\partial y^2}\right) \tag{2}$$

$$\rho_{ff}\left(\frac{\partial v}{\partial t}+u\frac{\partial v}{\partial x}+v\frac{\partial v}{\partial y}\right)=-\frac{\partial p}{\partial y}+\mu_{ff}\left(\frac{\partial^2 v}{\partial x^2}+\frac{\partial^2 v}{\partial y^2}\right)+(\rho_B)_{ff}g(T_{ff}-T_c)-\sigma_{ff}B^2v \tag{3}$$

$$(\rho C_p)_{ff}\left(\frac{\partial T_{ff}}{\partial t}+u\frac{\partial T_{ff}}{\partial x}+v\frac{\partial T_{ff}}{\partial y}\right)=k_{ff}\left(\frac{\partial^2 T_{ff}}{\partial x^2}+\frac{\partial^2 T_{ff}}{\partial y^2}\right) \quad \text{for the ferrofluid region} \tag{4}$$

$$(\rho C_p)_s\frac{\partial T_s}{\partial t}=k_s\left(\frac{\partial^2 T_s}{\partial x^2}+\frac{\partial^2 T_s}{\partial y^2}\right)+q'''_{gen} \quad \text{for the heat generating solid region} \tag{5}$$

Table 3
Comparison of present results for mean Nusselt number with the results of Calcagni et al. [53] for the case of square cavity model with $\varepsilon = 0.8$.

	$Ra = 10^4$	$Ra = 10^5$	$Ra = 10^6$
Calcagni et al. [53]	4.0	6.3	12.0
Present study	3.9767	6.4345	11.6673

Table 4
Total entropy production compared to data of Famouri and Hooman [25].

Ω	0.02	0.04	0.06	0.08	0.1
Famouri and Hooman [25]	6.701	6.576	6.457	6.342	6.231
Present study	6.7281	6.5991	6.4751	6.3558	6.2408

Table 5
Mesh sensitivity data for $\overline{Nu}$ at $Ra = 10^7$, $A_s = 1$, $k^* = 1$, $\varphi = 0.04$ and $Ha = 50$.

Grid	62 × 62	122 × 122	182 × 182	242 × 242
$\overline{Nu}$	12.2839	12.2467	12.2457	12.2415
$\lvert\Psi\rvert_{max}$	8.0831	7.9828	7.9658	7.9602

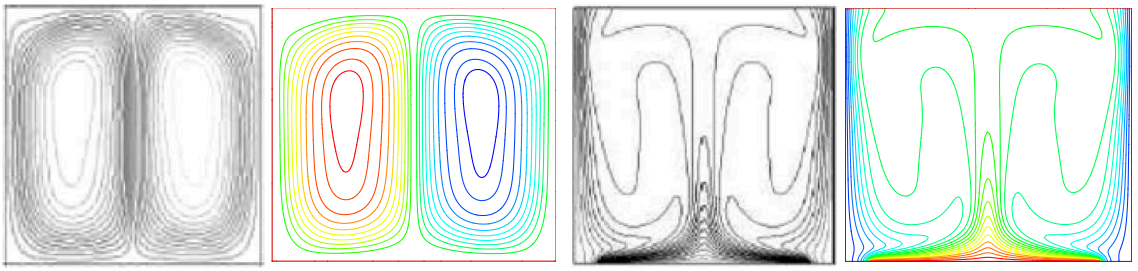

Fig. 3. Comparison of (left) experimental results of Calcagni et al. [53] and (right) present study. (a) Streamlines for $\varepsilon = 0.4$ and (b) isotherms for $\varepsilon = 0.8$ at $Ra = 10^6$.

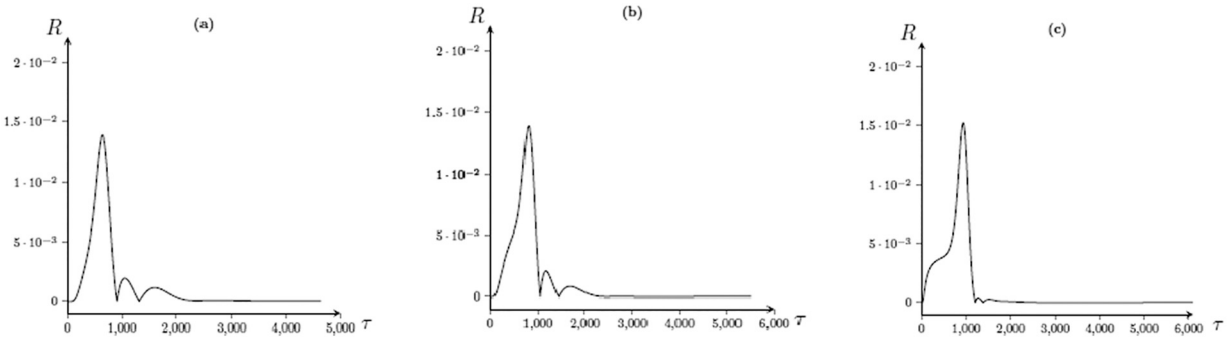

Fig. 4. Residual error plots with τ for $\varphi = 0.04$, $k^* = 1.0$ and $Ha = 50$. (a) $A_s = 0.25$, (b) $A_s = 1.0$ and $A_s = 4.0$.

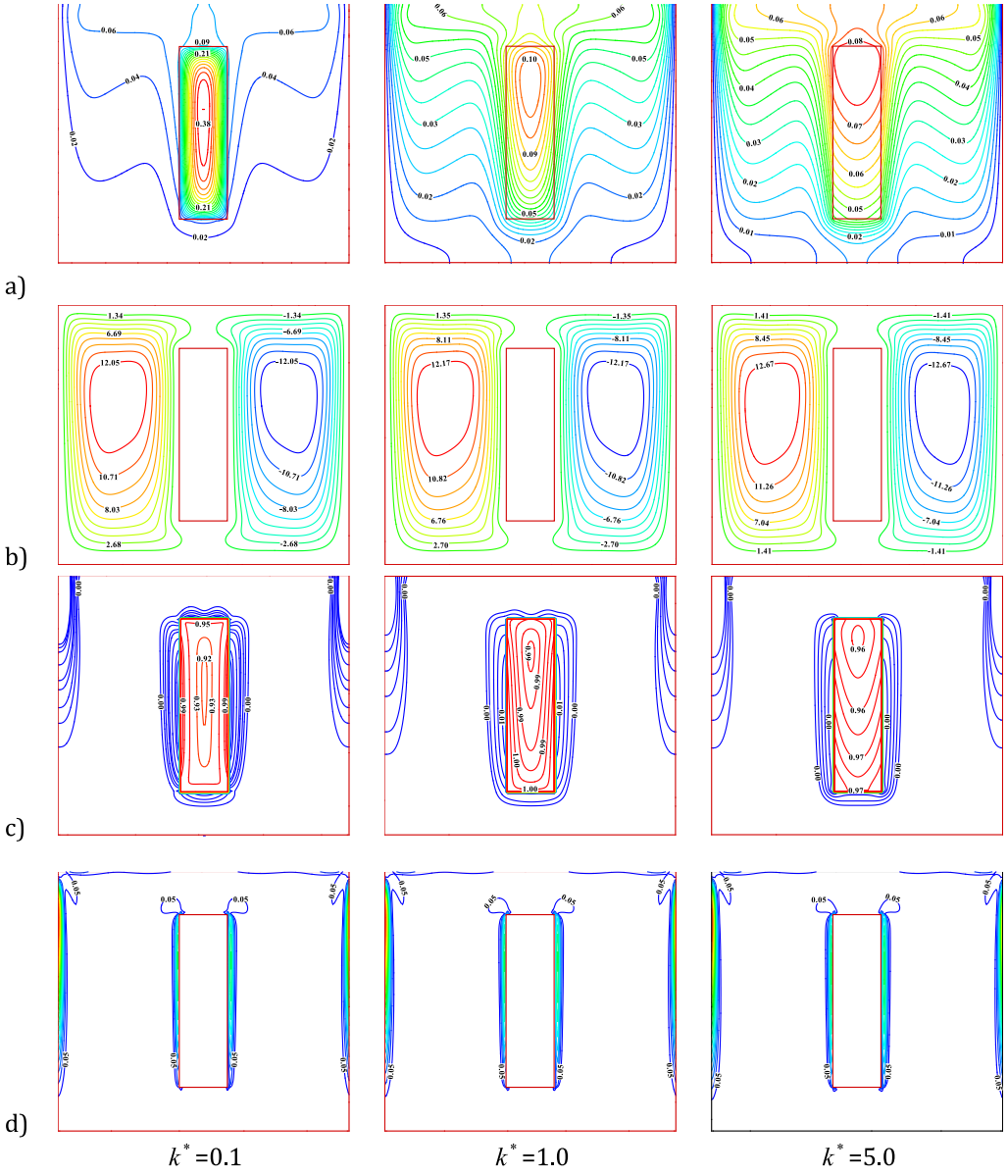

Fig. 5. (a) Isotherms, (b) streamlines, (c) entropy due to heat transference, and (d) entropy due to liquid friction at $A_s = 0.25$, $\Omega = 0.1$ and $Ha = 0$ for various k^*.

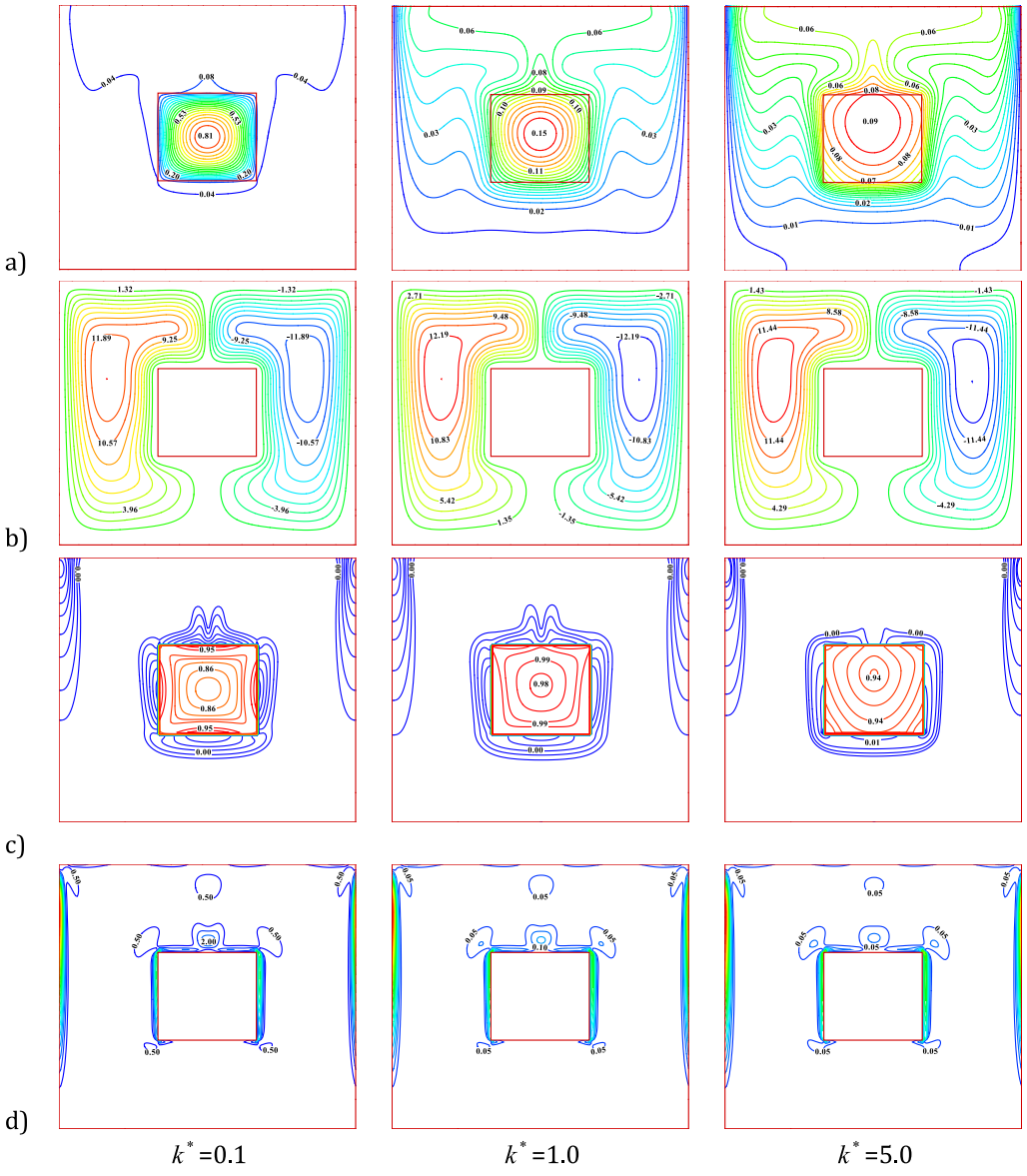

Fig. 6. (a) Isotherms, (b) streamlines, (c) entropy due to heat transference, and (d) entropy due to liquid friction at $A_s = 1.0$, $\Omega = 0.1$ and $Ha = 0$ for various k^*.

The following boundary conditions are involved in the present investigation as follows:

$$\begin{aligned} t = 0: &\quad u = v = 0, T_{\mathrm{ff}} = T_c, && \text{at } 0 \le x \le L \text{ and } 0 \le y \le L \\ t > 0: &\quad u = v = 0, T_{\mathrm{ff}} = T_c, && \text{at } x = 0, L \text{ and } 0 \le y \le L \\ &\quad u = v = 0, \frac{\partial T_{\mathrm{ff}}}{\partial y} = 0 && \text{at } y = 0, L \text{ and } 0 < x < L \\ &\quad u = v = 0, k_f \frac{\partial T_f}{\partial n} = k_s \frac{\partial T_s}{\partial n} && \text{at fluid/solid interfaces} \end{aligned} \tag{6}$$

The effective density, specific heat and thermal expansion coefficient of nanoliquid can be written as follows [43]:

$$\begin{aligned} \rho_{\mathrm{ff}} &= (1-\varphi)\rho_f + \varphi\rho_p, (\rho c_p)_{\mathrm{ff}} = (1-\varphi)(\rho c_p)_f + \varphi(\rho c_p)_p, (\rho\beta)_{\mathrm{ff}} \\ &= (1-\varphi)(\rho\beta)_f + \varphi(\rho\beta)_p \end{aligned} \tag{7}$$

The effective thermal conductivity of the nanoliquid defined using the Maxwell-Garnett [44] and Afrand [46,47] respectively:

$$\frac{k_{\mathrm{ff}}}{k_f} = \left\{ \frac{k_p + 2k_f - 2\varphi(k_f - k_p)}{k_p + 2k_f + \varphi(k_f - k_p)} \right\}; \frac{k_{\mathrm{ff}}}{k_f} = 0.9320 + 0.0673\varphi^{0.323} T^{0.245} \tag{8}$$

The standard effective viscosity given by Brinkmann [45] and a novel viscosity model given by Toghraie [48,49] are considered respectively:

$$\frac{\mu_{\mathrm{ff}}}{\mu_f} = \left\{ \frac{1}{(1-\varphi)^{2.5}} \right\}; \frac{\mu_{\mathrm{ff}}}{\mu_f} = [1.01 + (0.007165T^{1.171}\varphi^{1.509})\exp(-0.00719T\varphi)] \tag{9}$$

The effective electrical conductivity of the nanoliquid can be given by [34]

$$\frac{\sigma_{\mathrm{ff}}}{\sigma_f} = \left\{ \frac{\sigma_p + 2\sigma_f - 2\varphi(\sigma_f - \sigma_p)}{\sigma_p + 2\sigma_f + \varphi(\sigma_f - \sigma_p)} \right\} \tag{10}$$

There is an insignificant deviation between the novel model and standard model (See Fig. 2). The Maxwell and Brinkman mathematical models are adopted in this study.

To convert the governing equations into dimensionless form, we define the following the dimensionless variables and parameters [16]

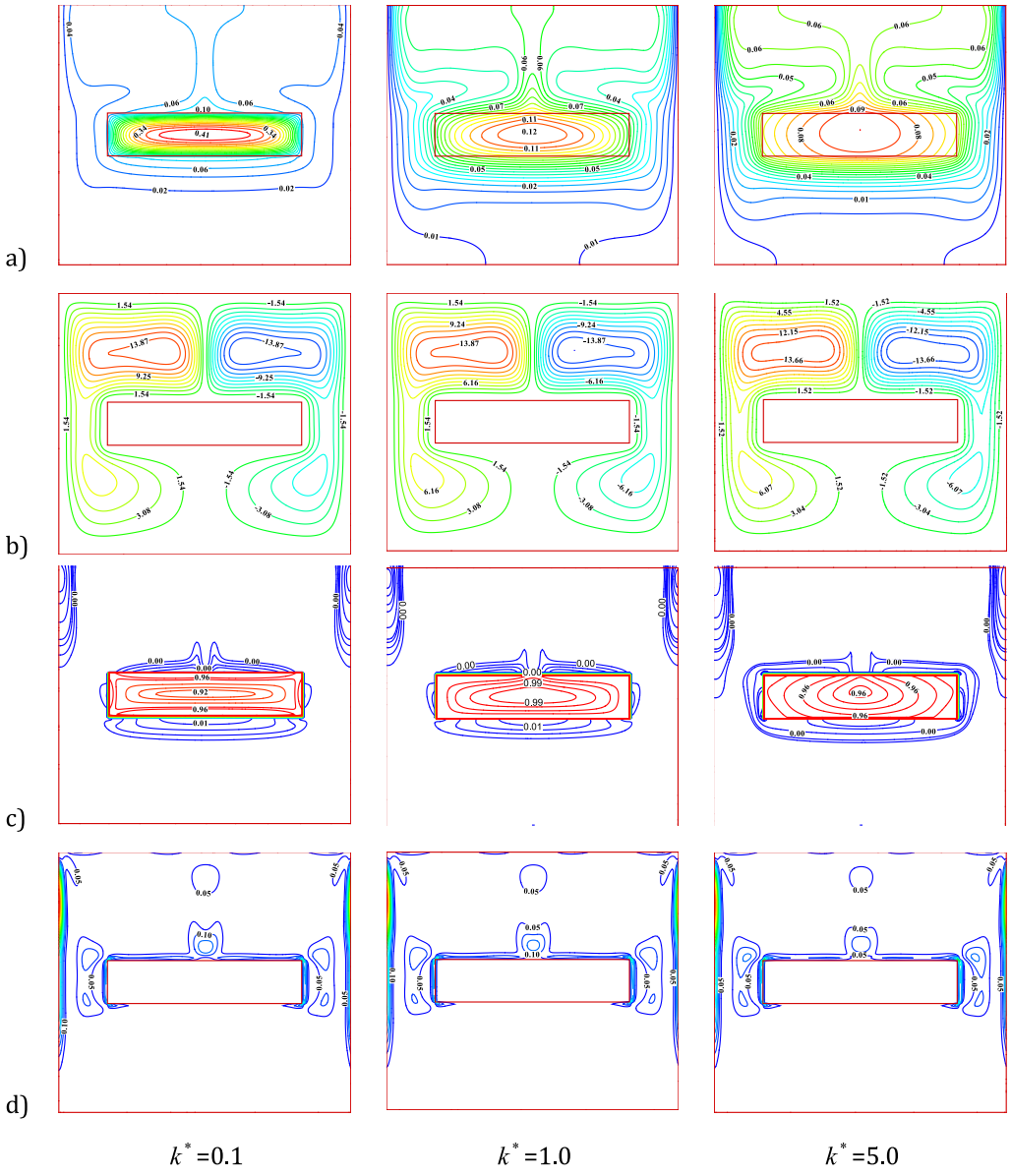

Fig. 7. (a) Isotherms, (b) streamlines, (c) entropy due to heat transference, and (d) entropy due to liquid friction at $A_s = 4.0$, $\Omega = 0.1$ and $Ha = 0$ for variousk^*.

$$X = \frac{x}{L}, Y = \frac{y}{L}, U = \frac{\mathrm{uL}}{\alpha_f}, V = \frac{\mathrm{vL}}{\alpha_f}, P = \frac{pL^2}{\rho_{\mathrm{ff}}\alpha_f^2}, \tau = \frac{t\alpha_f}{L^2}, \theta_{\mathrm{ff}} = \frac{T_{\mathrm{ff}} - T_c}{\Delta T},$$
$$\theta_s = \frac{T_s - T_c}{\Delta T}, \Delta T = \frac{q'''_{\mathrm{gen}} l_1 l_2}{k_f}, \mathrm{Pr} = \frac{\nu_f}{\alpha_f}, \mathrm{Ra} = \frac{g\beta_f \Delta T L^3}{\nu_f \alpha_f}, \mathrm{Ha} = \mathrm{BL}\sqrt{\frac{\sigma_f}{\mu_f}} \tag{11}$$

Thus, the governing equations can be written in dimensionless form as;

$$\frac{\partial U}{\partial X} + \frac{\partial V}{\partial Y} = 0, \tag{12}$$

$$\frac{\partial U}{\partial \tau} + U\frac{\partial U}{\partial X} + V\frac{\partial U}{\partial Y} = -\frac{\partial P}{\partial X} + \left(\frac{\mu_{\mathrm{ff}}}{\mu_f}\frac{\rho_f}{\rho_{\mathrm{ff}}}\right)\mathrm{Pr}\left(\frac{\partial^2 U}{\partial X^2} + \frac{\partial^2 U}{\partial Y^2}\right) \tag{13}$$

$$\frac{\partial V}{\partial \tau} + U\frac{\partial V}{\partial X} + V\frac{\partial V}{\partial Y} = -\frac{\partial P}{\partial Y} + \left(\frac{\mu_{\mathrm{ff}}}{\mu_f}\frac{\rho_f}{\rho_{\mathrm{ff}}}\right)\mathrm{Pr}\left(\frac{\partial^2 V}{\partial X^2} + \frac{\partial^2 V}{\partial Y^2}\right) + \left(\frac{(\rho\beta)_{\mathrm{ff}}}{\rho_{\mathrm{ff}}\beta_f}\right)\mathrm{Ra}\ \mathrm{Pr}\theta_{\mathrm{ff}} - \frac{\sigma_{\mathrm{ff}}}{\sigma_f}\frac{\rho_f}{\rho_{\mathrm{ff}}}\mathrm{Ha}^2\mathrm{Pr}\ \mathrm{V} \tag{14}$$

$$\frac{\partial \theta_{\mathrm{ff}}}{\partial \tau} + U\frac{\partial \theta_{\mathrm{ff}}}{\partial X} + V\frac{\partial \theta_{\mathrm{ff}}}{\partial Y} = \left(\frac{\alpha_{\mathrm{ff}}}{\alpha_f}\right)\left(\frac{\partial^2 \theta_{\mathrm{ff}}}{\partial X^2} + \frac{\partial^2 \theta_{\mathrm{ff}}}{\partial Y^2}\right) \quad \text{for the ferrofluid region} \tag{15}$$

$$\frac{\partial \theta_s}{\partial \tau} = \alpha * \left(\frac{\partial^2 \theta_s}{\partial X^2} + \frac{\partial^2 \theta_s}{\partial Y^2}\right) + \frac{1}{(\rho C_p) *}\frac{1}{A*} \quad \text{for the heat generating solid region} \tag{16}$$

with the corresponding boundary conditions

$$\begin{aligned}
\tau = 0: &\quad U = V = 0, \theta_{\mathrm{ff}} = 0 && \text{at } 0 \le X \le 1 \text{ and } 0 \le Y \le 1 \\
\tau > 0: &\quad U = V = 0, \theta_{\mathrm{ff}} = 0 && \text{at} X = 0, 1 \text{ and } 0 \le Y \le 1 \\
&\quad U = V = 0, \frac{\partial \theta_{\mathrm{ff}}}{\partial Y} = 0 && \text{at } Y = 0, 1 \text{ and } 0 < X < 1 \\
&\quad U = V = 0, \frac{\partial \theta_f}{\partial n} = k * \frac{\partial \theta_s}{\partial n} && \text{at fluid/solid interfaces}
\end{aligned} \tag{17}$$

Table 6
Maximum values of absolute stream function, temperature, local entropy production due to heat transference, liquid friction and magnetic field for $\Omega = 0.1$ and different A_s and Ha.

k^*	A_s	Ha	$\lvert\Psi\rvert_{max}$	θ_{max}	$S_{gen,HT,max}$	$S_{gen,FF,max}$	$S_{gen,MF,max}$
$k^* = 0.1$	0.25	$Ha = 0$	13.3842	0.3799	94.3697	1.365×10^{-6}	0.0
		Ha=50	7.3983	0.4038	94.1915	1.138×10^{-6}	3.584×10^{-7}
	1.0	Ha=0	13.2129	0.8142	98.7023	1.459×10^{-6}	0.0
		Ha=50	7.9165	0.8339	98.4575	1.202×10^{-6}	3.937×10^{-7}
	4.0	Ha=0	15.4124	0.4053	94.3276	1.673×10^{-6}	0.0
		Ha=50	8.5787	0.4221	94.2678	9.618×10^{-7}	3.485×10^{-7}
$k^* = 1.0$	0.25	$Ha = 0$	13.5216	0.1052	89.9925	1.367×10^{-6}	0.0
		Ha-50	7.4506	0.4038	89.8928	1.133×10^{-6}	3.596×10^{-7}
	1.0	Ha=0	13.5396	0.1504	90.3138	1.467×10^{-6}	0.0
		Ha=50	7.9658	0.1714	98.1281	1.194×10^{-6}	3.952×10^{-7}
	4.0	Ha=0	15.4071	0.1226	89.7850	1.692×10^{-6}	0.0
		Ha=50	8.6771	0.1387	89.8076	9.867×10^{-7}	3.575×10^{-7}
$k^* = 5.0$	0.25	$Ha = 0$	14.0759	0.0893	92.6558	1.358×10^{-6}	0.0
		Ha=50	7.6164	0.1087	93.5298	1.106×10^{-6}	3.583×10^{-7}
	1.0	Ha=0	14.2974	0.0977	95.3586	1.472×10^{-6}	0.0
		Ha=50	8.0181	0.1133	96.3949	1.169×10^{-6}	3.945×10^{-7}
	4.0	$Ha = 0$	15.1821	0.0919	92.9188	1.705×10^{-6}	0.0
		Ha=50	8.7070	0.1069	92.1269	9.926×10^{-7}	3.632×10^{-7}

where $A* = \frac{l_1 l_2}{L^2}; \alpha* = \frac{\alpha_s}{\alpha_f}; k* = \frac{k_s}{k_f}; (\rho C_p)* = \frac{(\rho C_p)_s}{(\rho C_p)_f};$

The fluid motion is displayed by means of stream function, which is acquired from velocity components U and V as follows

$$U = \frac{\partial \Psi}{\partial Y} \quad \text{and} \quad V = -\frac{\partial \Psi}{\partial X} \tag{18}$$

The local heat transfer rate at each surface of heat-generating body can be calculated from the following [16]

$$\mathrm{Nu} = \frac{k_{ff}\frac{\partial T_{ff}}{\partial n}}{k_f\frac{(T_{sf}-T_c)}{L}} = \frac{k_{ff}}{k_f}\frac{1}{\theta_{sf}}\frac{\partial \theta_{ff}}{\partial n} \tag{19}$$

To find the mean Nusselt number $(\overline{\mathrm{Nu}})$ at each surface of heat generating solid body, integration of their local analogues is utilized.

The volumetric rate of entropy generation due to temperature gradient can be expressed as [38]

$$s_{gen,HT} = s_{gen,HT,s} + s_{gen,HT,ff} \tag{20}$$

where

$$s_{gen,HT,s} = \frac{k_s}{T_s^2}\left[\left(\frac{\partial T_s}{\partial x}\right)^2 + \left(\frac{\partial T_s}{\partial y}\right)^2\right] + \frac{q'''_{gen}}{T_s} \quad \text{for heat generating solid region} \tag{21}$$

$$s_{gen,HT,ff} = \frac{k_{ff}}{T_{ff}^2}\left[\left(\frac{\partial T_{ff}}{\partial x}\right)^2 + \left(\frac{\partial T_{ff}}{\partial y}\right)^2\right] \quad \text{for ferrofluid region} \tag{22}$$

The volumetric rate of entropy generation due to viscous dissipation effect and external magnetic effect can be obtained as [27]

$$s_{gen,FF} = \frac{\mu_{ff}}{T_{ff}}\left[2\left(\frac{\partial u}{\partial x}\right)^2 + 2\left(\frac{\partial v}{\partial y}\right)^2 + \left(\frac{\partial u}{\partial y} + \frac{\partial v}{\partial x}\right)^2\right] \quad \text{and} \tag{23}$$

$$s_{gen,MF} = B^2\frac{\sigma_{ff}}{T_{ff}}v^2 \tag{24}$$

Introducing the following dimensionless local entropy generation (S_{gen}) [27],

$$S_{gen} = s_{gen}\frac{T_c^2 L^2}{k_f \Delta T^2} = S_{gen,HT} + S_{gen,FF} + S_{gen,MF} \tag{25}$$

The dimensionless local entropy generation due to heat transfer ($S_{gen,HT}$) is defined as follows:

$$S_{gen,HT} = S_{gen,HT,s} + S_{gen,HT,ff} \tag{26}$$

where the first term represents entropy due to heat transfer for a heat generating solid body and the second term denotes entropy due to heat transfer for the ferrofluid respectively.

$$S_{gen,HT,s} = \frac{k*}{\Omega^2(\theta_s + \Omega^{-1})^2}\left[\left(\frac{\partial \theta_s}{\partial X}\right)^2 + \left(\frac{\partial \theta_s}{\partial Y}\right)^2\right] + \frac{1}{\Omega^2(\theta_s + \Omega^{-1})}\frac{1}{A*} \tag{27}$$

$$S_{gen,HT,ff} = \frac{\left(\frac{k_{ff}}{k_f}\right)}{\Omega^2(\theta_{ff} + \Omega^{-1})^2}\left[\left(\frac{\partial \theta_{ff}}{\partial X}\right)^2 + \left(\frac{\partial \theta_{ff}}{\partial Y}\right)^2\right] \tag{28}$$

The dimensionless local entropy generation due to liquid friction ($S_{gen,FF}$) and local entropy generation due to magnetic field ($S_{gen,MF}$) is defined as:

$$S_{gen,FF} = \frac{\left(\frac{\mu_{ff}}{\mu_f}\right)}{\Omega^2(\theta_{ff} + \Omega^{-1})}\frac{\mathrm{Ge}}{\mathrm{Ra}}\left[2\left(\frac{\partial U}{\partial X}\right)^2 + 2\left(\frac{\partial V}{\partial Y}\right)^2 + \left(\frac{\partial U}{\partial Y} + \frac{\partial V}{\partial X}\right)^2\right] \tag{29}$$

$$S_{gen,MF} = \frac{\left(\frac{\sigma_{ff}}{\sigma_f}\right)}{\Omega^2(\theta_{ff} + \Omega^{-1})}\frac{\mathrm{Ge}}{\mathrm{Ra}}\mathrm{Ha}^2 V^2 \tag{30}$$

where the dimensionless irreversibility ratio (Ω) and the Gebhart number (Ge) are defined as:

$$\Omega = \frac{\Delta T}{T_c} \quad \text{and} \quad \mathrm{Ge} = \frac{g\beta_f L}{(c_p)_f} \tag{31}$$

Gebhart number is a dimensionless number representing the effect of viscous dissipation in thermal convection, which plays a pivotal role as it comes to studying second law of the thermodynamics aspects of a convection problem. Gebhart number (Ge) is defined as the ratio of the kinetic energy of the flow to the heat transferred to the fluid. Gebhart number can be calculated via Rayleigh number (Ra), irreversibility ratio (Ω) by setting up cold wall temperature as $T_c = 300K$.

The integration of Eq. (25) in the entire computational domain gives the dimensionless mean entropy production ($S_{T,Avg}$) expressed as follows:

$$S_{T,Avg} = \int_A S_{gen}\mathrm{d}A = S_{HT,Avg} + S_{FF,Avg} + S_{MF,Avg} \tag{32}$$

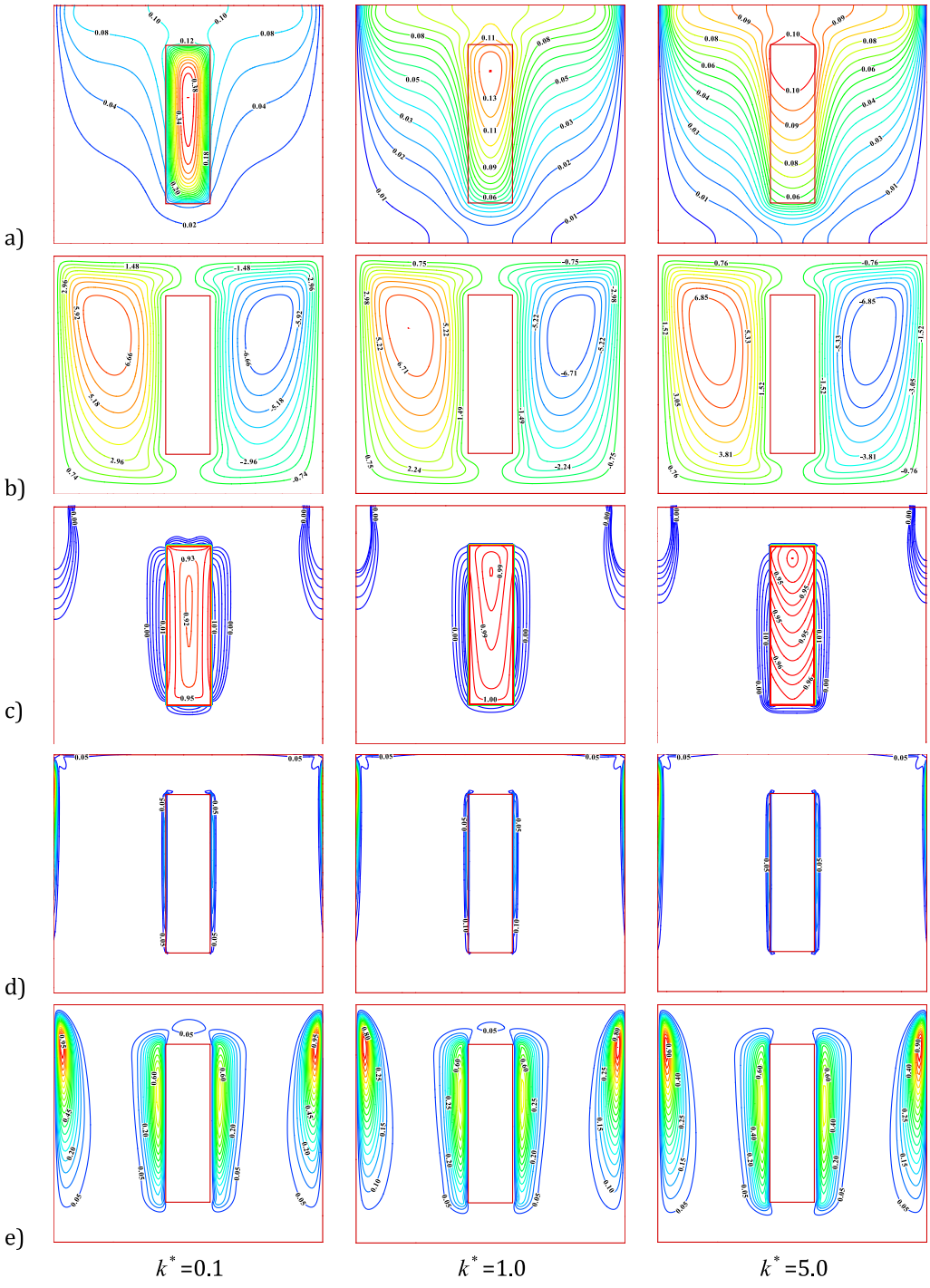

Fig. 8. (a) Isotherms, (b) streamlines, (c) entropy due to heat transference, (d) entropy due to liquid friction and (e) entropy due to magnetic effect at $A_s = 0.25$, $\Omega = 0.1$ and $Ha = 50$ for variousk^*.

$$\mathrm{Be}_{\mathrm{Avg}} = \frac{S_{\mathrm{HT,Avg}}}{S_{\mathrm{HT,Avg}} + S_{\mathrm{FF,Avg}} + S_{\mathrm{MF,Avg}}} = \frac{S_{\mathrm{HT,Avg}}}{S_{T,\mathrm{Avg}}} \tag{33}$$

3. Computational technique and validation

The dimensionless governing equations are worked out by using the control volume method with the simple algorithm procedure of Patankar [51] on a uniform staggered grid to attain the numerical simulations in a ferrofluid-filled square chamber. Time term is treated using the forward difference approach and the pressure - velocity field in the momentum equations are coupled together under relaxation technique, whereas convective and diffusive terms are handled by using third-order QUICK scheme of Hayase et al [52] and the second-order central difference scheme respectively. The iterative process is executed by a line-by-line procedure tri-diagonal matrix algorithm (TDMA) algorithm. The time step is assumed to be 10^{-3} and the convergence criterion of the sequential iterative solution is given below:

$$\frac{\sum_{i,j}|\zeta_{i,j}^{m} - \zeta_{i,j}^{m-1}|}{\sum_{i,j}|\zeta_{i,j}^{m}|} \leq 10^{-7} \tag{34}$$

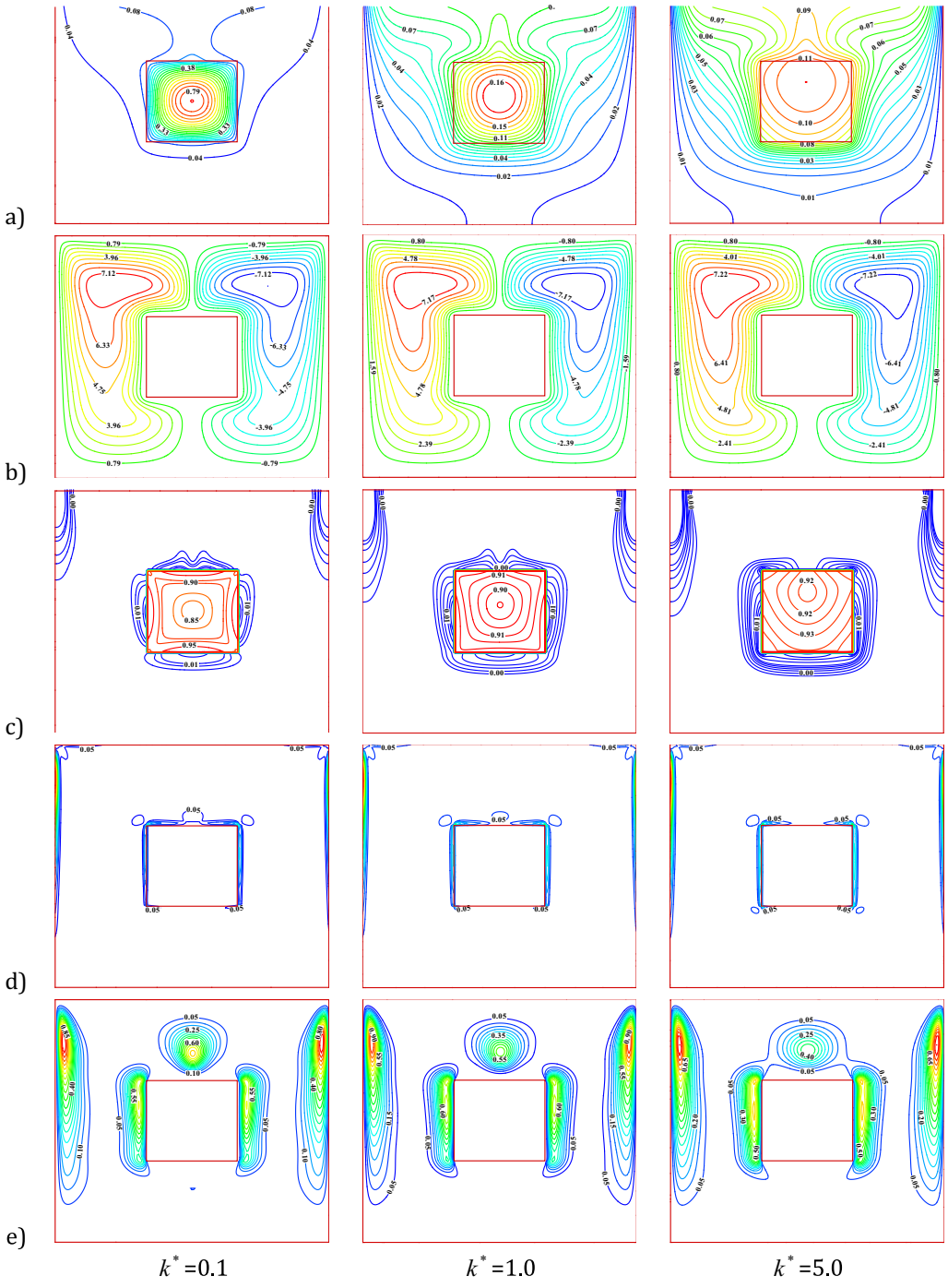

Fig. 9. (a) Isotherms, (b) streamlines, (c) entropy due to heat transference, (d) entropy due to liquid friction and (e) entropy due to magnetic effect at $A_s = 1.0$, $\Omega = 0.1$ and $Ha = 50$ for various k^*.

Here ζ represents the variables U, V and θ, the superscript m and subscript (i, j) refer the iteration number and the space coordinates, respectively.

An agreement between the results provides assurance in the accurateness of the existing code to explore the formulated problem. To validate the numerical data of the current work, a comparison was made with data of House et al. [1] shown in Table 2. In order to test the accuracy of the present numerical code, the obtain figures were compared with the prevailing experimental results of Calcagni et al. [53] for the case of thermal convective heat transfer in a square chamber which is heated from below, as shown in Fig. 3 and Table 3. Further, to validate the numerical data of the current work, a comparison was made with data of Famouri and Hooman [25] presented in Table 4.

Also, the mesh sensitivity was investigated by employing four grids of 62×62, 122×122, 182×182 and 242×242. The mean Nusselt number $(\overline{Nu})$ and maximum value of stream function $(|\Psi|_{max})$ for each case are examined. From Table 5, it can be observed that data do not have essential differences between the successive grids and established that the grid size of 182×182 is appropriate for all further computations with an optimal time. The residual errors with dimensionless time for different aspect ratios are plotted in Fig. 4, and it is ascertained that the

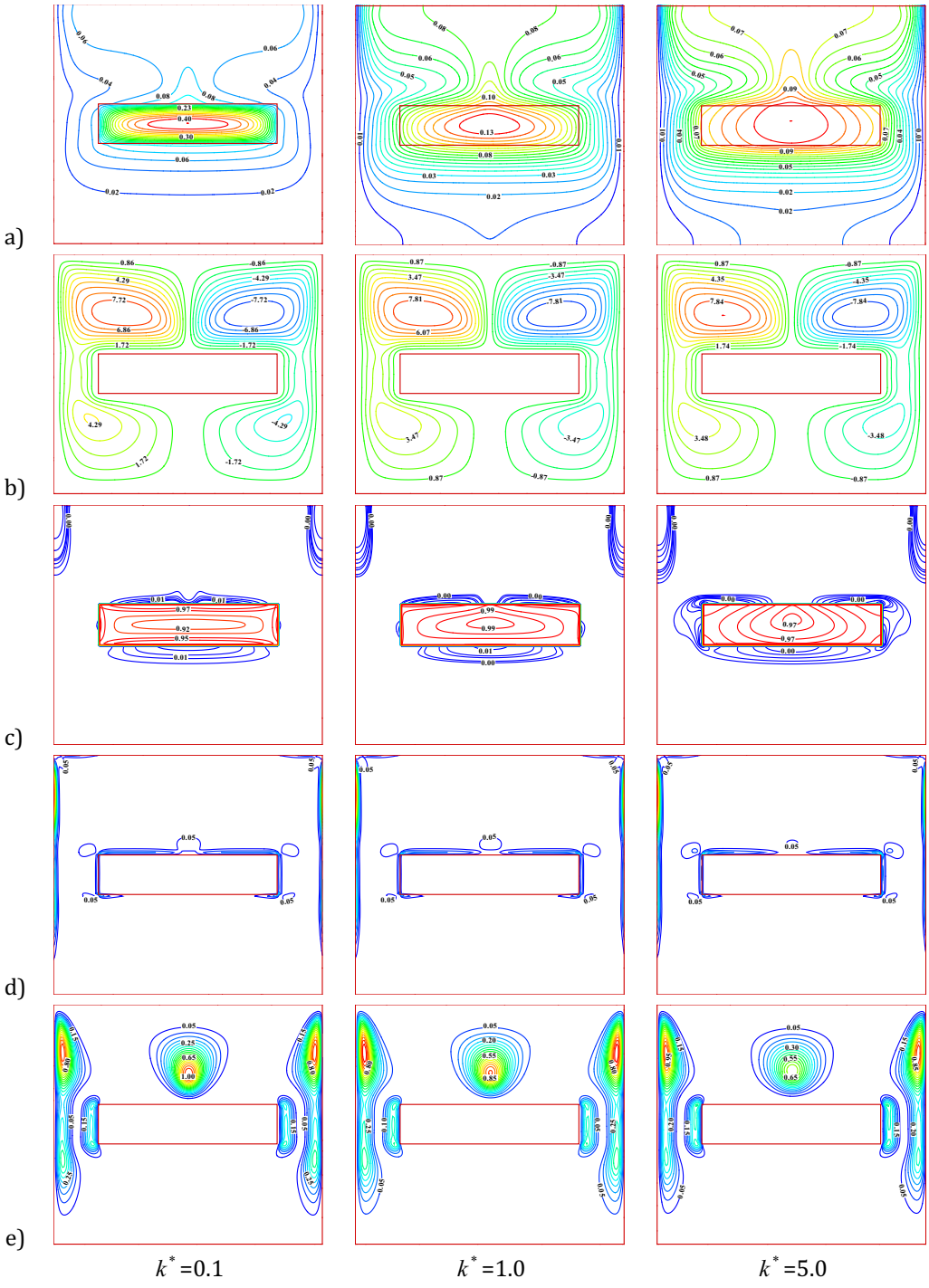

Fig. 10. (a) Isotherms, (b) streamlines, (c) entropy due to heat transference, (d) entropy due to liquid friction and (e) entropy due to magnetic effect at $A_s = 4.0$, $\Omega = 0.1$ and $Ha = 50$ for various k*.

acquired solution is accurate; consequently, it converges well for the designated value of the pertinent parameters that are concerned in the governing control equations.

4. Results and discussion

The numerical simulations are executed to establish heat and flow features in a square chamber with heat-generating solid body with various aspect ratio. Ferrofluid consists of magnetite nanoadditive, which is suspended in a host liquid (water) and becomes strongly magnetized when subjected to a magnetic field. So, prominent thermo-magnetic convection will occur when an external magnetic field is imposed on a ferrofluid. Ferrofluid is employed in this work and computations have been conducted for $Pr = 6.8377$ and $(\rho C_p)^* = 1$. The area ratio of the solid body A^* is fixed as 1/9 while the length and width of the solid body is varied i.e., aspect ratio $(0.25 \le A_s \le 4)$. Variations of the operating parameters are considered, namely, thermal conductivity ratio parameter $(0.1 \le k^* \le 5.0)$, magnetic field $(0 \le Ha \le 50)$, and irreversibility ratio $(0.001 \le \Omega \le 0.1)$. As such, the Gebhart number (Ge) was calculated through the parameters, Ra, Ω and $T_c = 300K$. For presumed values of $Ra = 10^7$, $L \approx 2.9cm$, $q'''_{gen} \approx 197\text{kW/m}^3$ and $\Omega = 0.1$, Gebhart number takes the value 1.41×10^{-8}. Further Ge takes

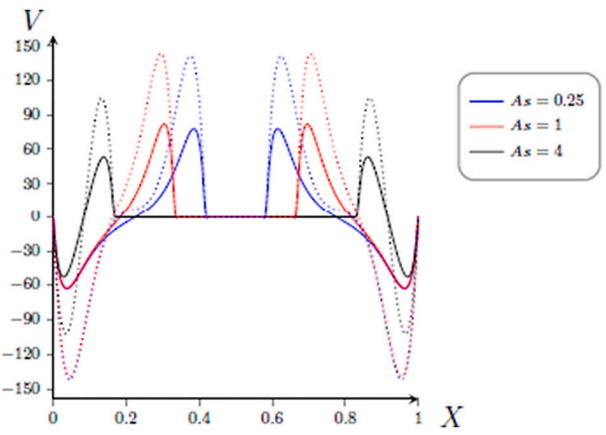

Fig. 11. Vertical mid-height velocity for $\varphi = 0.04$, $k^* = 1.0$ with different A_s and Ha. $Ha = 0$ (dotted lines), $Ha = 50$ (solid lines).

the value 3.03×10^{-8} for $\Omega = 0.01$ and 6.53×10^{-8} for $\Omega = 0.001$ respectively. The results obtained from the current simulations are presented in terms of streamlines, temperature, and entropy contours. The local entropy contours are plotted using normalized values, which can be easily found by dividing corresponding value by the maximum local entropy generation.

4.1. Flow field and temperature distributions

Figs. 5–7 (a-b) shows the isolines of temperature and stream function as influenced by the aspect ratio variations as well as thermal conductivity ratio. For all aspect ratio, it is observed that the structure of the thermal and fluid flow fields is symmetric with respect to the vertical mid-line of the cavity. This can be explained by symmetrical boundary conditions of the cooled vertical walls. Moreover, the crowded isotherm patterns close to the heat-generating body point out the higher magnitude of temperature gradients prevailing there which in turn produce the thermal plume over the heat-generating solid body. When k^* =0.1, the isotherms are densely packed only within the inner heat generating

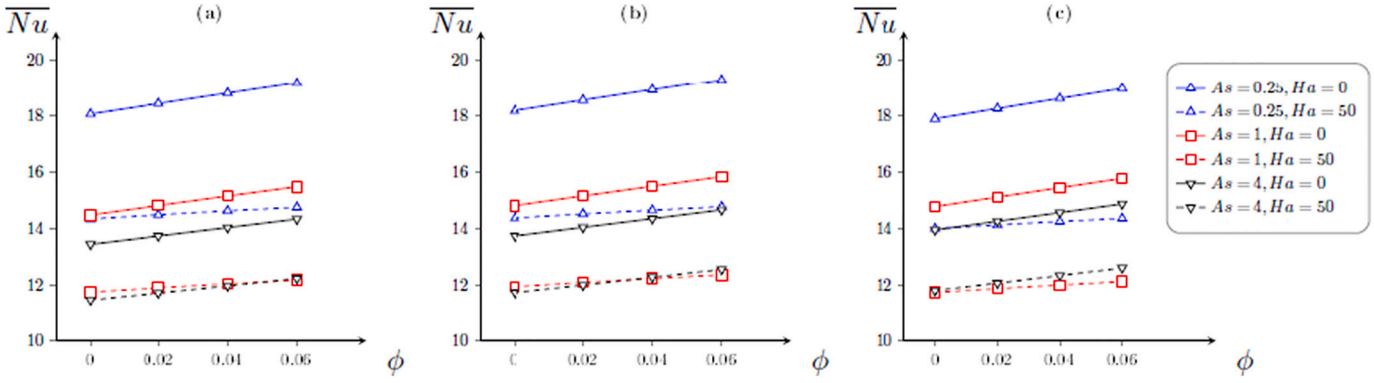

Fig. 12. Mean Nusselt number at $\Omega = 0.1$ with different φ, A_s, Ha and for different k^*. (a) $k^* = 0.1$, (b) $k^* = 1$, and (c) $k^* = 5$.

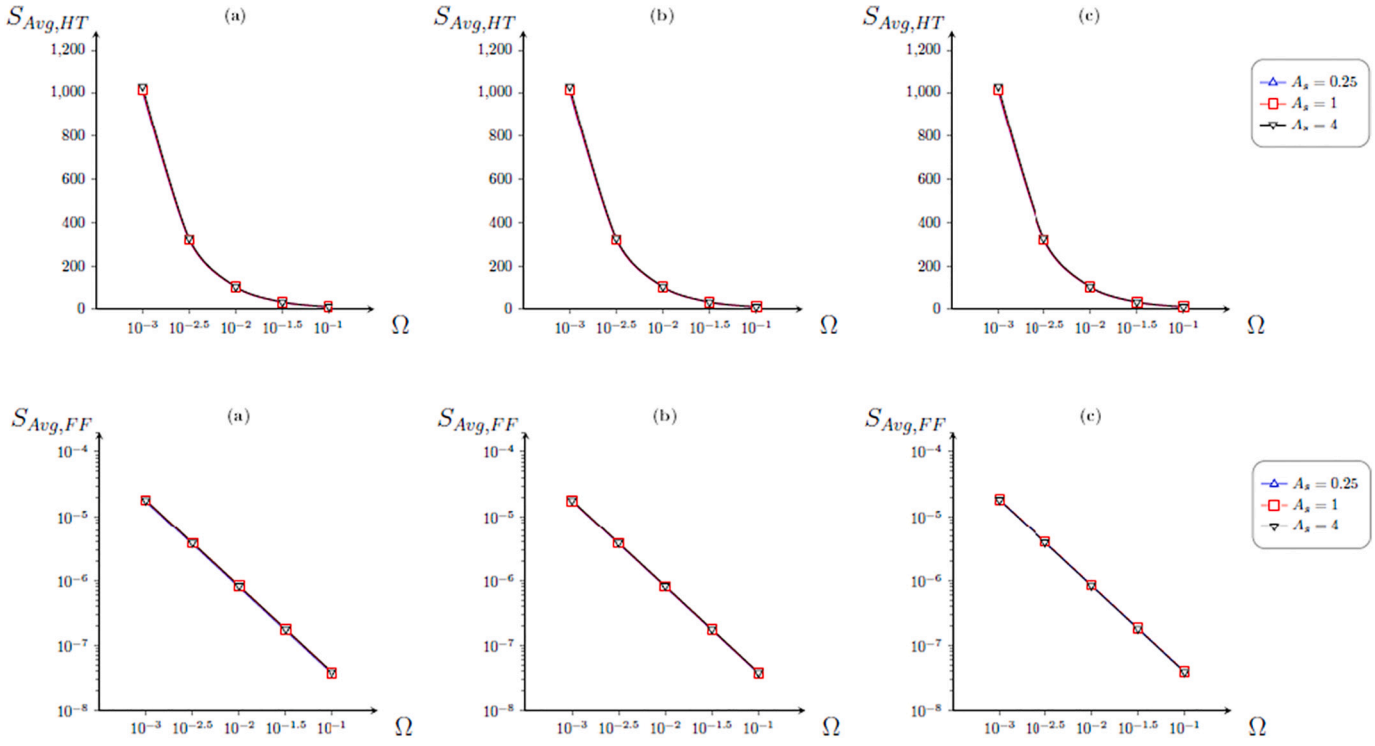

Fig. 13. Mean entropy due to heat transference and liquid friction with $\overline{Nu}$ and $S_{T,Avg} = 0$ for various A_s and k^*. (a) $k^* = 0.1$, (b) $k^* = 1.0$ and (c) $k^* = 5.0$.

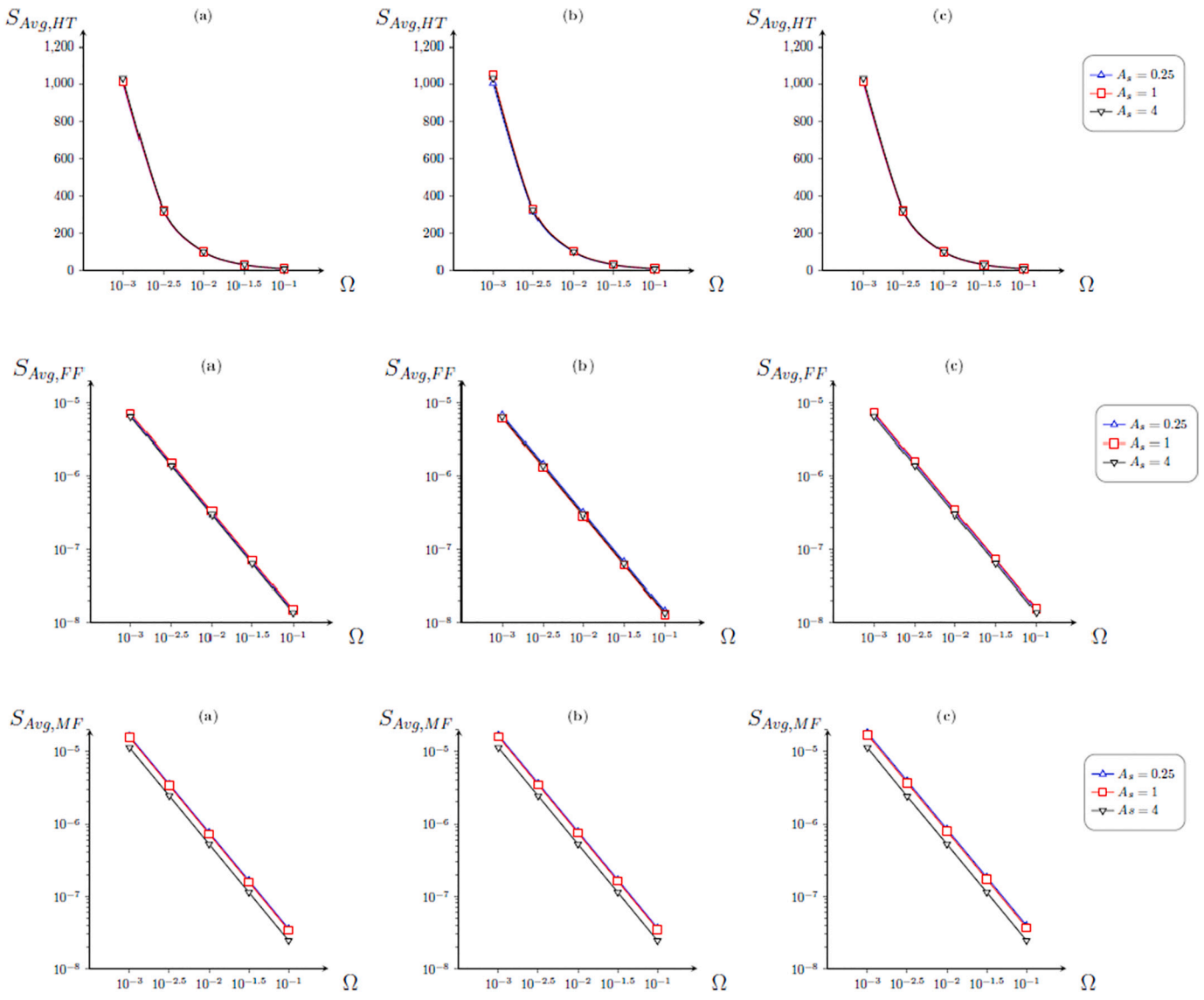

Fig. 14. Mean entropy due to heat transference, liquid friction and magnetic effect with Ω and $Ha = 50$ for various A_s and k*. (a) $k^* = 0.1$, (b) $k^* = 1.0$ and (c) $k^* = 5.0$.

Table 7
Mean Nusselt number, total entropy generation and thermal performance criteria for $\Omega = 0.1$ and different A_s and Ha.

k^*	A_s	$\overline{Nu}$	$S_{T,Avg}$	TPC (ε)	$\overline{Nu}$	$S_{T,Avg}$	TPC (ε)
			$Ha = 0$			$Ha = 50$	
	0.25	18.7926	10.0881	0.5368	14.6306	10.0899	0.6897
$k^* = 0.1$	1.0	15.1531	10.1711	0.6721	12.0593	10.1728	0.8436
	4.0	14.0422	10.3364	0.7361	11.9878	10.3374	0.8623
	0.25	18.9151	10.0887	0.5334	14.6544	10.0905	0.6886
$k^* = 1.0$	1.0	15.4983	10.1722	0.6563	12.2457	10.5044	0.8578
	4.0	14.3568	10.3379	0.7201	12.2877	10.3388	0.8414
	0.25	18.6029	10.0897	0.5423	14.2549	10.0920	0.7079
$k^* = 5.0$	1.0	15.4469	10.1765	0.6588	12.0174	10.1796	0.8471
	4.0	14.5672	10.3435	0.7101	12.3498	10.3439	0.8376

solid body due to the conduction effect inside the heat-generating solid block. As conductivity ratio (k *) increases, the amount of heat transferred from the heat generating solid body to the nanofluid is increased so that isotherms get less intensified at the central region of the solid body. Additionally, thermal boundary layer appears over the surface of the solid body and along the top surface of chamber cold walls. Another important remark is that occurrence of minimum θ_{max} at the middle of the heat-generating solid body indicating a uniform cooling effect from all sides and the better convective cooling corresponding to solid body happening with $A_s = 0.25$.

The corresponding fluid flow pattern is demonstrated by two symmetric counter-rotating strong convective cells both rising at the vertical

surface of the solid body and falling along the vertical boundaries of the cavity. Symmetrically imposed boundary conditions are responsible for this symmetric structure. The heat-generating solid body and vertical cold walls are account for strong clockwise and anticlockwise convective cells with centered cores at each part of the chamber. When $A_s = 0.25$, fluid particles move around liberally due to hindrance-free configuration and buoyant effect. One can find that the vortices are produced at each side of the cavity and it elongates in a vertical direction. As aspect ratio increases, interference of solid obstruction accountable for the convection flow on the upper domain and conduction effect on the lower domain. A further increase in A_s creates an obstruction effect in downward fluid motion results in the reduction of fluid velocity. Even though an increase in k^* characterizes the different intensity of the considered process with higher momentum (see $|\Psi|_{max}$ values from Table 6).

4.2. Entropy contours

The principal objective of engineers is not only finding an effective cooling configuration also to design the thermal system from energy-saving point of view. This can be achieved by analyzing entropy production. Figs. 5–7 (c-d) demonstrates the irreversibility due to heat transference and liquid friction for different values of A_s and k^*. In general, entropy generation due to heat transference is always characterized by temperature gradient and it is highly concentrated at the surfaces of the thermally-producing solid body, while it is less concentrated at the top of the vertical wall. The remaining area acts as almost entropy-free zones due to the cooling effect of ferric-oxide nanoliquid. The temperature gradient at the surfaces of the solid block is maximum, which is owing to the boundary layer regime. This is generated due to the reason that the liquid next to the heat generating solid body acquires heat and becomes very lighter, which impels the heat towards the heat-generating solid block. This recurrence process results in maximum entropy along the surfaces of heat-generating solid body, thereby this regime in reality, represents the energy loss zone. With further increase of the k^* value, entropy production due to heat transference increases more because of the steeper temperature gradient at the heat generating solid body. Therefore, the maximum thermal entropy production is happening at the surfaces of the heat-generating solid body for all aspect ratio.

The entropy production due to liquid friction characterizes the velocity gradient. It is concentrated on the vertical walls and vertical surface of the heat-generating solid body due to the occurrence of velocity boundary layers. Also, frictional entropy vortices above the solid body and the top corners of the chamber can be found due to the interaction of high-velocity recirculation cells, which is responsible for a significant velocity gradient. We can also observe that the existence of buoyancy force occurring at the edges of the heat-generating solid body and frictional force at the interacting edges of the counter-rotating cells produces the entropy lines at those regions.

4.3. Fluid flow and temperature distributions due to magnetic effect

Figs. 8–10 (a-b) shows the variations of the aspect ratio, thermal conductivity ratio on isolines, and stream function as influenced by the magnetic field. The Lorentz force within the enclosure is introduced, the flow velocity of the nanoliquid is decreased. As the aspect ratio increased, it is seen from isotherms that the inclusion of magnetic field in the horizontal direction creates the Lorentz force in the orthogonal direction resist the heat transfer and makes the upper part of the cavity more thermally active with a significant thermal boundary layer thickness. In common, more isotherms stick out the flat face of the heat-generating solid body. Heat dissipation will happen through the faces of heat-generating solid body, which is affected by Lorenz force signifying a sparse distribution of temperature contours. In particular, increasing the thermal conductivity ratio, the isotherms get less intensified with more uniform at the central region and its surrounding region due to the high thermal conductivity of solid body it conducts heat from solid to the fluid. In general, the magnetic effect also allows the maximum temperature to occur at the core of heat-generating solid body.

When the magnetic field is applied horizontally, the strength of the convective flow in the cavity gets weakened and significant changes in the vortex shape are observed. Since, the Lorentz force creates more attenuation effect in the vertical flow, shifting the core region of vortices and thus the deviated fluid particles fall smoothly along the vertical walls with the thin momentum boundary layer near the vertical boundaries. Upon increasing the aspect ratio, due to the obstruction effect, it is found that effective convective cells are formed in the upper cavity and weak convective cells are formed in the lower cavity that suppresses the fluid flow rate. As Ha is increased, the secondary cells are formed with in the cavity.

There is no disparity in the streamlines for the rest of thermal conductivity ratio. It was shown that growth of Ha leads to an essential diminution of the strength of liquid motion within the enclosure. Particularly, in the absence of a magnetic field, an increase in a ferrofluid circulation rate $|\Psi|_{max,Ha=0} = 13.5396 > |\Psi|_{max,Ha=50} = 7.9658$ was witnessed for $\varphi = 0.04$. Increasing the thermal conductivity ratio results in the increase of flow motion strength can be explained by higher momentum values. (see $|\Psi|_{max}$ values from Table 6).

4.4. Entropy contours due to magnetic field

Figs. 8–10 (c-e) shows entropy due to heat transfer, liquid friction, and magnetic field respectively. Entropy generation due to energy transport demonstrates that effective entropy contours are extremely noticeable near the surface of the heat-generating solid body where the temperature gradient is maximum that can be seen in Figs. 8–10 (c). The heat from the solid interacts with nanoliquid, which impulse the heat towards the heat solid body constantly. As a result, the magnetic field impedes convection current for all aspect ratio. The energy loss is gradually enhanced with increasing the k^* value from 0.1 to 5. In that way, entropy generation due to heat transfer dominates more because of the steeper thermal gradient around the heat-generating solid body.

Figs. 8-10 (d) depicts the influence of magnetic field on entropy production due to liquid friction inside the chamber for various A_s and k^*. The inclusion of the magnetic field reduces the fluid friction entropy lines due to less velocity gradient. By increasing of number, a reduction in velocity can be observed. It can be seen from the mid-height vertical velocity profiles for $Ha = 0$ and $Ha = 50$ (see Fig. 11). The fluid flow along the vertical walls and vertical surfaces of the obstruction experiences the effects of the attenuation from the Lorentz force, which produces low thickness of velocity boundary layers and hence more fluid friction entropy lines there. As such, the vertical surface of the solid body and the upper part of the vertical chamber characterizes significant velocity gradients. When A_s increases additional liquid friction entropy contours appear near the upper horizontal surface of the heat-generating solid body and a remaining core region act as entropy free zones. It is reasoned that the high interruption of the solid body slows down the fluid velocity within the cavity and hence reduces the velocity gradients. As increasing the aspect ratio, entropy generation due to liquid friction decreases. As a result, the overall energy of the fluid drastically reduces under the influence of Lorentz force. There is an insignificant reduction in the entropy production as the thermal conductivity ratio changes its value from 0.1 to 5.0.

Figs. 8–10 (e) displays the local entropy contours owing to the magnetic influence. A growth of Hartmann number boosts magnetic entropy production. Since the magnetic field is applied in the horizontal direction, the intensity of Lorentz force is higher in the vertical direction and lower in the horizontal direction. For the minimum value of aspect ratio, magnetic entropy contours occur near to the vertical surface of both the solid body and boundaries. When the aspect ratio increased, the highest rate of magnetic entropy production occurs above the solid body

where recirculating convective cells occur due to extended interference and Lorentz force. For minimal thermal conductivity ratio, magnetic entropy production is fewer and also recognized that the dominance of irreversibility is heat transfer irreversibility.

4.5. Heat transfer rate

The mean Nusselt Number is an increasing function of nano-additive concentration due to the enhanced thermal conductivity of nanoliquid. We observe that for a fixed aspect ratio, the mean *Nu* is monotonically increasing relation of φ in the case of magnetic inclusion as well. It is reasoned that the addition of nano additives to the base fluid improves both the thermal conductivity and effective viscosity of a nanoliquid. Moreover, addition of magnetic field ($Ha = 50$), the effect of Lorentz force controls the heat transfer process in the entire cavity leads to suppress the convective heat transfer process. Thus, the mean Nusselt number is reduced. This is clearly seen in Fig. 12. Mean *Nu* reduces with an increase of the aspect ratio of heat-generating solid body. It is presumed that increasing aspect ratio values result in a slowdown of the heat transfer process. We also found that among the different aspect ratios of the solid body considered $A_s = 0.25$ makes the maximum *Nu* in the presence of magnetic field effect. It should be mentioned that an increase in k^* contributes to slight growth of the mean Nusselt number for both the case of magneto and non-magneto-convective thermal transmission. It can be characterized by the heat transferred from the solid surface to the fluid and increases the fluid temperature.

4.6. Irreversibility analysis

Figs. 13 and 14 show the profiles of mean entropy production for both magnetic and non-magnetic cases. Entropy production drops as the ΔT rise due to its inverse proportionality. $S_{gen,HT}$, $S_{gen,FF}$ and $S_{gen,MF}$ are caused by a temperature gradient, velocity gradient, and magnetic field respectively. The addition of the Lorentz effect reflects an enhancement of mean entropy due to heat transfer. Moreover, this Lorentz force produces no significant changes in the parameters of the entropy caused by liquid friction and magnetic field. As the aspect ratio of the heat-generating solid body grows, the irreversibility caused by heat transfer will take a larger area near the solid body. From the observation, the mean entropy production is maximum for the aspect ratio ($A_s = 4$) and minimum for the aspect ratio ($A_s = 0.25$) . Entropy production is taken into consideration to opt for the desirable values of k^* and A_s. For a minimum value of thermal conductivity ratio, the entropy production due to heat transfer is lesser than the other cases. $Be \approx 1$, since there exists insignificant liquid friction and magnetic entropy compared to thermal entropy production. In other words, entropy production due to heat transfer dominates the entire domain.

A thermal performance criterion (TPC) is an important parameter which provides maximum heat transfer with minimum input of work, i.e., minimum thermodynamic irreversibility. Therefore, establishing a ratio of the total entropy generation to the mean Nusselt number noticeably addresses the feature of such performance. ε-criterion [54]:

$$\mathrm{TPC}(\varepsilon) = \frac{\mathrm{EG}}{\mathrm{HT}} = \frac{S_{T,\mathrm{Avg}}}{\overline{\mathrm{Nu}}} \tag{35}$$

According to the definition, minimal epsilon value gives better performance. Since the epsilon (ε) is directly proportional to entropy production and inversely proportional to heat transfer and the corresponding TPC is presented in Table 7. For a fixed k^*, an increase in aspect ratio results in high thermal performance criteria, meanwhile, an increase in *Ha* results in high thermal performance criteria. As k^* increases, there exists no linearity in epsilon criteria. In thermal performance point of view, the value of $A_s = 0.25$ manifests the best performance characterized by minimum entropy production, maximum heat transfer and the minimal epsilon criterion.

5. Conclusion

This study examines MHD thermal convection and entropy production inside a square chamber filled with ferrofluid having a heat generating solid block. The energy equation is formulated in both the fluid and solid media and is solved simultaneously with momentum and mass equations using a finite volume technique. The impact of the aspect ratio of the solid block, nano-additives, magnetic effect, thermal conductivity ratio, and irreversibility ratio on the comprehensive thermal performance was explained through numerical simulation. The main conclusions are summarized below.

- The study shows that heat transfer is improved when the volume fraction of nanoliquid increases. To obtain maximum cooling, the aspect ratio of the heat generating solid body must be smaller and heat transfer will be enhanced.
- Appliance of a uniform magnetization has the effect to limit the flow of nanoliquid into the chamber. The mean *Nu* reduces as the Hartmann number grows, which is caused by the Lorentz effect. The maximum heat transfer rate occurs at a high thermal conductivity ratio; meanwhile, minimum entropy production occurs at a low thermal conductivity ratio.
- The heat-generating solid body with the aspect ratio ($A_s = 0.25$) and low thermal conductivity ($k^* = 0.1$) is most desirable as this configuration produces minimum irreversibility.
- The new criterion for thermal performance determines the ratio of the thermodynamic irreversibility to the convective heat transfer. Achieving optimal TPC has more advantages at the lower values of A_s for all the cases are justified.
- This discussion is limited to the magnetic effect applied horizontally; by studying the various types of effects such as radiation effect and an inclined magnetic effect, the research findings may be helpful as guidance for further research into the thermal performance. Further, the cavity inclining by an angle can be generalized in the simulations.

Declaration of Competing Interest

The authors declare no conflict of interest.

Acknowledgements

This work of C. Sivaraj was carried out as a part of a research project (Grant No: INT/RUS/RFBR/P-282) awarded by the Department of Science and Technology, India.

References

[1] J.M. House, C. Beckermann, T.E. Smith, Effect of a centered conducting body on natural convection heat transfer in an enclosure, Numer. Heat Trans. Part A 18 (1990) 213–225.
[2] J.Y. Oh, M.Y. Ha, K.C. Kim, Numerical study of heat transfer and flow of natural convection in an enclose with a heat generating conducting body, Numer. Heat Trans. Part A 31 (1997) 289–303.
[3] M.Y. Ha, M.J. Jung, Y.S. Kim, Numerical study on transient heat transfer and fluid flow of natural convection in an enclosure with a heat-generating conducting body, Numer. Heat Trans. Part A 35 (1999) 415–433.
[4] I.V. Miroshnichenko, M.A. Sheremet, H.F. Oztop, N. Abu-Hamdeh, Natural convection of Al_2O_3/H_2O nanofluid in an open inclined cavity with a heat-generating element, Int. J. Heat Mass Trans. 126 (2018) 184–191.
[5] D.S. Bondarenko, M.A. Sheremet, H.F. Oztop, M.E. Ali, Natural convection of Al_2O_3/H_2O nanofluid in a cavity with a heat-generating element, Heatline visualization, Int. J. Heat Mass Trans. 130 (2019) 564–574.
[6] A. Nouar, A. Dib, M. Kezzar, M.R. Sari, M.R. Eid, Numerical treatment of squeezing unsteady nanofluid flow using optimized stochastic algorithm, Zeitschrift fur Naturforschung (2021), https://doi.org/10.1515/zna-2021-0163.
[7] A. Karimipour, S.A. Bagherzadeh, M. Goodarzi, A.A. Alnaqi, M. Bahiraei, M. R. Safaei, M.S. Shadloo, Synthesized $CuFe_2O_4/SiO_2$ nanocomposites added to water/EG: evaluation of the thermophysical properties beside sensitivity analysis & EANN, Int. J. Heat Mass Trans. 127 (2018) 1169–1179.

[8] S.A. Bagherzadeh, A. D'Orazio, A. Karimipour, M. Goodarzi, Q.V. Bach, A novel sensitivity analysis model of EANN for F-MWCNTs-Fe_3O_4/EG nanofluid thermal conductivity: Outputs predicted analytically instead of numerically to more accuracy and less costs, Physica A 521 (2019) 406–415.

[9] A. Shahsavar, S.K. Mohammadi, A. Karimipour, M. Goodarzi, A novel comprehensive experimental study concerned synthesizes and prepare liquid paraffin Fe_3O_4mixture to develop models for both thermal conductivity & viscosity: a new approach of GMDH type of neural network, Int. J. Heat Mass Trans. 131 (2019) 432–441.

[10] H.R. Goshayeshi, M. Goodarzi, M. Dahari, Effect of magnetic field on the heat transfer rate of kerosene/Fe_2O_3 nanofluid in a copper oscillating heat pipe, Exp. Therm. Fluid Sci. 68 (2015) 663–668.

[11] H.R. Goshayeshi, M. Goodarzi, M.R. Safaei, M. Dahari, Experimental study on the effect of inclination angle on heat transfer enhancement of a ferrofluid in a closed loop oscillating heat pipe under magnetic field, Exp. Therm. Fluid Sci. 74 (2016) 265–270.

[12] H.R. Goshayeshi, M.R. Safaei, M. Goodarzi, M. Dahari, Particle size and type effects on heat transfer enhancement of Ferro-nanofluids in a pulsating heat pipe, Powder Technol. 301 (2016) 1218–1226.

[13] S. Saravanan, C. Sivaraj, Combined thermal radiation and natural convection in a cavity containing a discrete heater: Effects of nature of heating and heater aspect ratio, Int. J. Heat Fluid Flow 66 (2017) 70–82.

[14] S.A. Mikhailenko, M.A. Sheremet, A.A. Mohamad, Convective-radiative heat transfer in a rotating square cavity with a local heat-generating source, Int. J. Mech. Sci. 142-143 (2018) 530–540.

[15] E.V. Shulepov, M.A. Sheremet, H.F. Oztop, N. Abu-Hamdeh, Mixed convection-radiation in lid driven cavities with nanofluids and time-dependent heat-generating body, J. Therm. Anal. Calorim. 146 (2020) 725–738.

[16] C. Sivaraj, I.V. Miroshnichenko, M.A. Sheremet, Influence of thermal radiation on thermogravitational convection in a tilted chamber having heat-producing solid body, Int. Commun. Heat Mass Trans. 115 (2020) 104611.

[17] M.F. Nia, A.B. Ansari, S.A. Gandjalikhan Nassab, Transient combined volumetric radiation and free convection in a chamber with a hollow heat-generating solid body, Int. Commun. Heat Mass Trans. 119 (2020) 104937.

[18] M.R. Eid, M.A. Nafe, Thermal conductivity variation and heat generation effects on magneto-hybrid nanofluid flow in a porous medium with slip condition, Waves Rand. Comp. Media (2020), https://doi.org/10.1080/17455030.2020.1810365.

[19] B.M. Amine, F. Redouane, L. Mourad, W. Jamshed, M.R. Eid, W. Al-Kouz, Magnetohydrodynamics natural convection of a triangular cavity involving Ag–MgO/Water hybrid nanofluid and provided with rotating circular barrier and a quarter circular porous medium at its Right-angled corner, Arab. J. Sci. Eng. (2021), https://doi.org/10.1007/s13369-021-06015-6.

[20] W. Jamshed, M.R. Eid, K.S. Nisar, N.A.A. Mohd Nasir, A. Edacherian, C. Ahamed Saleel, V. Vijayakumar, A numerical frame work of magnetically driven Powell-Eyring nanofluid using single phase model, Scientific Rep. (2021), 11:16500.

[21] M.R. Eid, K.L. Mahny, A.F. Al-Hossainy, Homogeneous-heterogeneous catalysis on electromagnetic radiative Prandtl fluid flow: darcy-forchheimer substance scheme, Surf. Interf. 24 (2021) 101119.

[22] C.M. Ayeche, M. Kezzar, M.R. Sari, M.R. Eid, Analytical ADM study of time-dependent hydromagnetic flow of biofluid over a wedge, Ind. J. Phys. (2021), https://doi.org/10.1007/s12648-020-01935-9.

[23] T. Tayebi, H.F. Oztop, A.J. Chamkha, MHD natural convection of a CNT-based nanofluid-filled annular circular enclosure with inner heat-generating solid cylinder, Eur. Phys. J. Plus 136 (2021) 150.

[24] S.Z. Shuja, M.O. Iqbal, B.S. Yilbas, Natural convection in a square cavity due to a protruding body - aspect ratio consideration, Heat Mass Trans. 37 (2001) 361–369.

[25] M. Famouri, K. Hooman, Entropy generation for natural convection by heated partitions in a cavity, Int. Commun. Heat Mass Trans. 35 (2008) 492–502.

[26] M. Sheikholeslami, H.R. Ashorynejad, P. Rana, Lattice boltzmann simulation of nanofluid heat transfer enhancement and entropy generation, J. Mol. Liq. 214 (2016) 86–95.

[27] C. Sivaraj, M.A. Sheremet, MHD natural convection and entropy generation of ferrofluids in a cavity with a non-uniformly heated horizontal plate, Int. J. Mech. Sci. 149 (2018) 326–337.

[28] A.A. Alnaqi, S. Aghakhani, A.H. Pordanjani, R. Bakhtiari, A. Asadi, M.D. Tran, Effects of magnetic field on the convective heat transfer rate and entropy generation of a nanofluid in an inclined square cavity equipped with a conductor fin: Considering the radiation effect, Int. J. Heat Mass Trans. 133 (2019) 256–267.

[29] A.A.A. Al-Rashed, Investigating the effect of alumina nanoparticle on heat transfer and entropy generation inside a square enclosure equipped with two inclined blades under magnetic field, Int. J. Mech. Sci. 152 (2019) 312–328.

[30] D.S. Bondarenko, M.A. Sheremet, H.F. Oztop, M.E. Ali, Impacts of moving wall and heat-generating element on heat transfer and entropy generation of Al_2O_3/H_2O nanofluid, J. Therm. Anal. Calorim. 136 (2019) 673–686.

[31] T. Tayebi, A.J. Chamkha, Entropy generation analysis during MHD natural convection flow of hybrid nanofluid in a square cavity containing a corrugated conducting block, Int. J. Numer. Methods Heat Fluid Flow 30 (2019) 1115–1136.

[32] R. Parveen, T.R. Mahapatra, Numerical simulation of MHD double diffusive natural convection and entropy generation in a wavy enclosure filled with nanofluid with discrete heating, Heliyon 5 (2019) e02496.

[33] Z. Li, A.K. Hussein, O. Younis, M. Afrand, S. Feng, Natural convection and entropy generation of a nanofluid around a circular baffle inside an inclined square cavity under thermal radiation and magnetic field effects, Int. Commun. Heat Mass Trans. 116 (2020) 104650.

[34] C. Sivaraj, S. Priyadharsini, M.A. Sheremet, Thermal convection and entropy generation of ferrofluid in an enclosure containing a solid body, Int. J. Numer. Methods Heat. Fluid Flow 31 (2020) 2940–2961.

[35] O. Cicek, A.C. Baytas, Conjugate forced convection in a semi-cylindrical cavity with entropy generation, Int. J. Numer. Methods Heat Fluid Flow 30-8 (2020) 3879–3902.

[36] O. Cicek, A.F. Baytas, A.C. Baytas, Entropy generation of mixed convection of SWCNT-water nanofluid filled an annulus with a rotating cylinder and porous lining under LTNE, Int. J. Numer. Methods Heat Fluid Flow 31-5 (2021) 1588–1617.

[37] C. Sivaraj, V.E. Gubin, A.S. Matveev, M.A. Sheremet, Impacts of uniform magnetic field and internal heated vertical plate on Ferrofluid free convection and entropy generation in a square chamber, Entropy 23 (2021) 70.

[38] S.R. Hosseini, M. Ghasemian, M. Sheikholeslami, A. Shafee, Z. Li, Entropy analysis of nanofluid convection in a heated porous microchannel under MHD field considering solid heat generation, Powder Technol. 344 (2019) 914–925.

[39] M.R. Eid, M.A. Ali, A.F. Al-Hossainy, Experimental characterization, TDDFT–DFT, and spin effect on $[PEG/H_2O - ZrO_2/TiO_2]_h$ hybrid nanofluid 3D flow as potential ceramic industry application, Int. J. Chem. React. Eng. (2021), https://doi.org/10.1515/ijcre-2021-0124.

[40] A.F. Al-Hossainy, M.R. Eid, Combined theoretical and experimental DFT–TDDFT and thermal characteristics of 3-D flow in rotating tube of $[PEG + H_2O/SiO_2 - Fe_3O_4]_C$ hybrid nanofluid to enhancing oil extraction, Waves Rand. Comp. Media (2021), https://doi.org/10.1080/17455030.2021.1948631.

[41] W. Jamshed, K.S. Nisar, R.W. Ibrahim, F. Shahzad, M.R. Eid, Thermal expansion optimization in solar aircraft using tangent hyperbolic hybrid nanofluid: a solar thermal application, J. Mater. Res. Technol. 14 (2021) 985–1006.

[42] W. Jamshed, M.R. Eid, N.A.A. Mohd Nasir, K.S. Nisar, A. Aziz, F. Shahzad, C. Ahamed Saleel, A. Shukla, Thermal examination of renewable solar energy in parabolic trough solar collector utilizing Maxwell nanofluid: a noble case study, Case Stud. Thermal. Eng. 27 (2021) 101258.

[43] S. Malik, A.K. Nayak, MHD convection and entropy generation of nanofluid in a porous enclosure with sinusoidal heating, Int. J. Heat Mass Trans. 111 (2017) 329–345.

[44] J.C. Maxwell, A Treatise on Electricity and Magnetism, Oxford University Press, Cambridge, 1904, pp. 435–441.

[45] H.C. Brinkman, The viscosity of concentrated suspensions and solutions, J. Chem. Phys. 20 (4) (1952) 571–581.

[46] M. Molana, R. Ghasemiasl, T. Armaghani, A different look at the effect of temperature on the nanofluids thermal conductivity: focus on the experimental-based models, J. Therm. Anal. Calorim. (2021), https://doi.org/10.1007/s10973-021-10836-w.

[47] M. Afrand, D. Toghraie, N. Sina, Experimental study on thermal conductivity of water-based Fe_3O_4 nanofluid: development of a new correlation and modeled by artificial neural network, Int. Commun. Heat Mass Trans. 75 (2016) 262–269.

[48] A. Barkhordar, R. Ghasemiasl, T. Armaghani, Statistical study and a complete overview of nanofluid viscosity correlations: a new look, J. Therm. Anal. Calorim. (2021), https://doi.org/10.1007/s10973-021-10993-y.

[49] D. Toghraie, S.M. Alempour, M. Afrand, Experimental determination of viscosity of water based magnetite nanofluid for application in heating and cooling systems, J. Magnet. Mag. Mater. 417 (2016) 243–248.

[50] L. Wang, Y. Wang, X. Yan, X. Wang, B. Feng, Investigation on viscosity of Fe_3O_4 nanofluid under magnetic field, Int. Commun. Heat Mass Trans. 7 (2016) 23–28.

[51] S.V. Patankar, Numerical Heat Transfer and Fluid flow, Hemisphere Publishing Corporation, New York, 1980.

[52] T. Hayase, J.A.C. Humphrey, R. Greif, A consistently formulated QUICK scheme for fast and stable convergence using finite-volume iterative calculation procedures, J. Comput. Phys. 98 (1992) 108–118.

[53] B. Calcagni, F. Marsili, M. Paroncini, Natural convective heat transfer in square enclosures heated from below, Appl. Therm. Eng. 25 (2005) 2522–2531.

[54] M.A. Ismael, T. Armaghani, A.J. Chamkha, Conjugate heat transfer and entropy generation in a cavity filled with a nanofluid-saturated porous media and heated by a triangular solid, J. Taiwan Inst. Chem. Eng. 59 (2016) 138–151.